Antibacterial surfaces bearing copper nanoparticles on titanium implants

Maria G. Sande

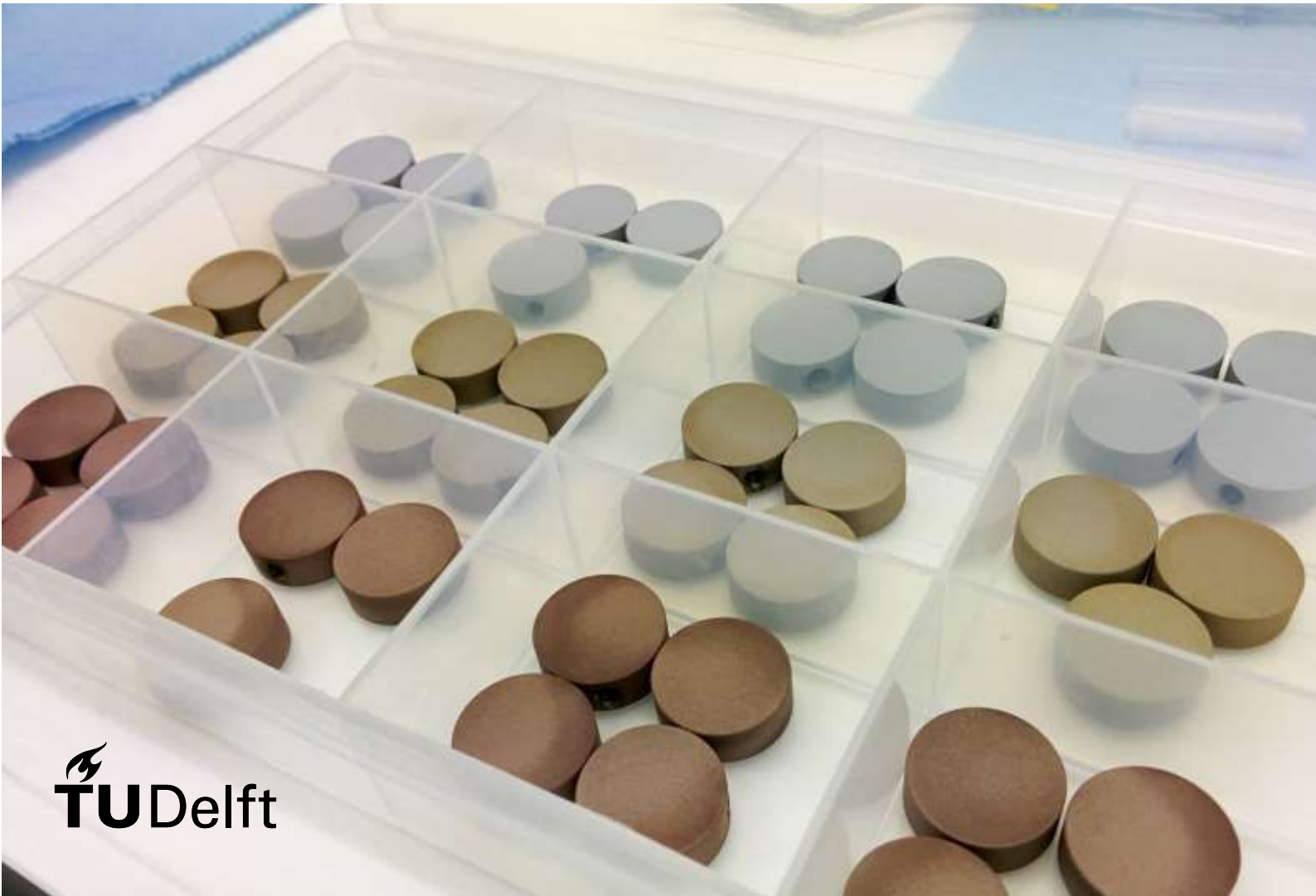

TU Delft

Antibacterial surfaces bearing copper nanoparticles on titanium implants

By

Maria G. Sande

in partial fulfilment of the requirements for the degree of

Master of Science
in Biomedical Engineering

at the Delft University of Technology,
to be defended publicly on Wednesday November 30, 2016 at 12:00 PM.

Supervisors: Dr. ir. I. Apachitei
Dr. ir. A.A Zadpoor

Biomaterials and Tissue Biomechanics Section
Biomechanical Engineering Department
Faculty of Mechanical, Maritime and Materials Engineering
Delft University of Technology

Contents

Abstract

Bacterial infection is one of the most severe complications of titanium based implants which leads to complete implant failure. The treatment of such infections requires multiple surgeries followed by long term antibiotic therapies with significant traumatic consequences to patients and high financial burden for healthcare systems.

One option to increase the resistance of titanium implants to bacterial infection is to create an antimicrobial layer on the implant surface without affecting its biocompatibility. Ag based antimicrobial surfaces are currently studied with good antimicrobial activity against multidrug resistant bacteria (e.g. Methicillin-resistant Staphylococcus aureus - MRSA). However silver proved to induce quite strong cytotoxic effect to host cells which may impede the osseointegration process of titanium bone implants. Recently it has been shown that Cu ions (Cu^{2+}) seem to be suitable both to kill specific bacteria and stimulate biological responses like cell proliferation and osteogenic differentiation. Therefore incorporation of Cu nanoparticles on a TiO_2 surface that can release Cu^{2+} at the implant-tissue interface may lead to a new generation of Ti implants with dual functionalities i.e. bactericidal and osteoconductive. Plasma electrolytic oxidation (PEO) is a surface modification technique that enables incorporation of Cu nanoparticles into a porous TiO_2 layer. Furthermore, this technique is suitable to cover complex implant geometries such as hip or knee components.

Cu-bearing TiO_2 layers were synthesised by PEO on Ti6Al7Nb biomedical alloy and characterised by scanning electron microscopy (SEM), energy dispersive X-ray spectroscopy (EDS) and X-ray diffraction (XRD). The analyses revealed that the TiO_2 layers were rough, completely covered with interconnected micro pores and Cu nanoparticles had been successfully incorporated into the surface. Inductively Coupled Plasma-Optical Emission Spectrometry (ICP-OES) analysis was used to quantify the release of Cu^{2+} from the surface of Cu-bearing layers into phosphate-buffered saline (PBS) media. Cu^{2+} showed sustained release over a period of sixty days.

A direct contact assay was used to assess the *in vitro* surface antibacterial activity of the Cu-bearing TiO_2 layers against specific concentrations of *S. aureus* and MRSA bacterial species. Both bacterial species were completely killed after 24 hours. An agar diffusion assay was used to study the leachable antibacterial activity of the Cu-bearing TiO_2 layers against *S. aureus.* A bacterial growth inhibition zone was observed around the sample disc indicating Cu had an at least bacteriostatic effect against bacteria-containing agar. Overall, Cu-bearing layers displayed good antibacterial activity against the pathogen which is the most common cause of bacterial infection in implants (*S. aureus*) and against a virulent multi-drug resistant pathogen (MRSA). The release of Cu^{2+} into PBS coupled with the inhibition of bacterial growth by Cu-bearing TiO_2 layers suggest that a sustained antibacterial effect of Cu-bearing TiO_2 layers is possible which could extend to its surroundings.

1 Introduction

1.1. Osteoarthritis and implant associated infections

1.1.1 Treatment of osteoarthritis

Osteoarthritis is a degenerative joint disorder mainly characterized by the deterioration of articular cartilage on the ends of bones in normal joints (Fig. 1.1). People suffering with advanced cases of osteoarthritis experience chronic pain, tenderness and stiffness in the joints along with loss of flexibility of the affected limbs. Worldwide it affects 9.6% of men and 18.0% of women over the age of 60, making it the single most common cause of disability among older adults [1]. There is no cure at present for osteoarthritis but it is routinely treated by total joint replacement (TJR) surgery in which the damaged joint is replaced with an artificial joint called an implant (Fig. 1.2). TJR surgery restores function of affected joints to some extent and greatly relieves pain in most cases [2].

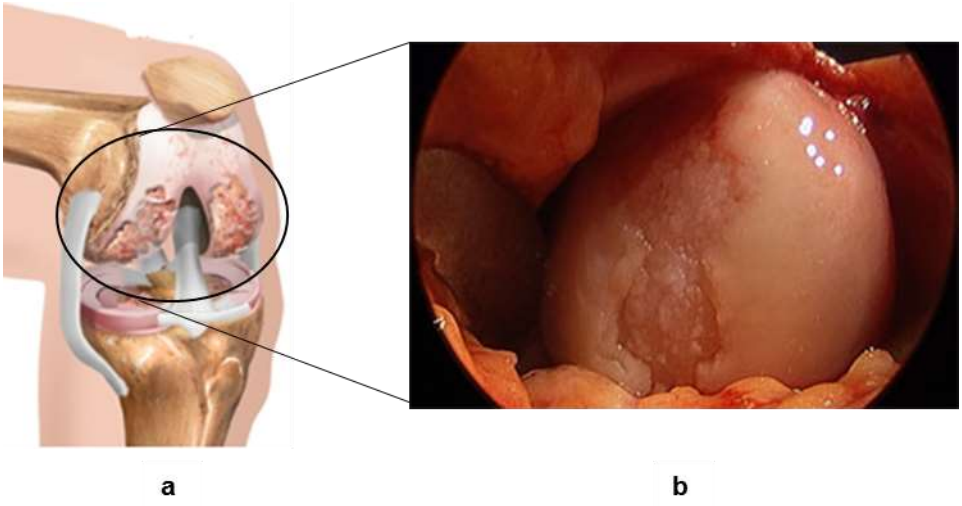

Figure 1.1. A representation of an osteoarthritic knee joint showing damage to cartilage caused by osteoarthritis (a) and a close up image of the damaged cartilage revealing wear and exposure of subchondral bone (b) [3].

One of the major challenges had been the development of permanent, stable methods to affix an implant to bone. There are two fixation methods for implants at present: (i) mechanical fixation of the implant to the bone using polymethylmethacrylate (PMMA), also called bone cement and (ii) biological fixation achieved through bone ingrowth into the implant surface and osseointegration [4]. Implants for which bone cement is used are called cemented implants. These implants are usually made of cobalt chromium alloys which has good biocompatibility. The major disadvantage of cemented implants is that osseointegration is not possible leading to cases of aseptic loosening. Cementless implants are ususally made from titanium alloys such as Ti6Al4V and more recently, Ti6Al7Nb. The major advantage of titanium-based implants is that direct intimate contact of the implant surface with the host bone, among other factors, provide the conditions for

osseointegration to occur. The porous implant surface facilitates ingrowth of bone into the implant leading to good stability and subsequently long life of the implant.

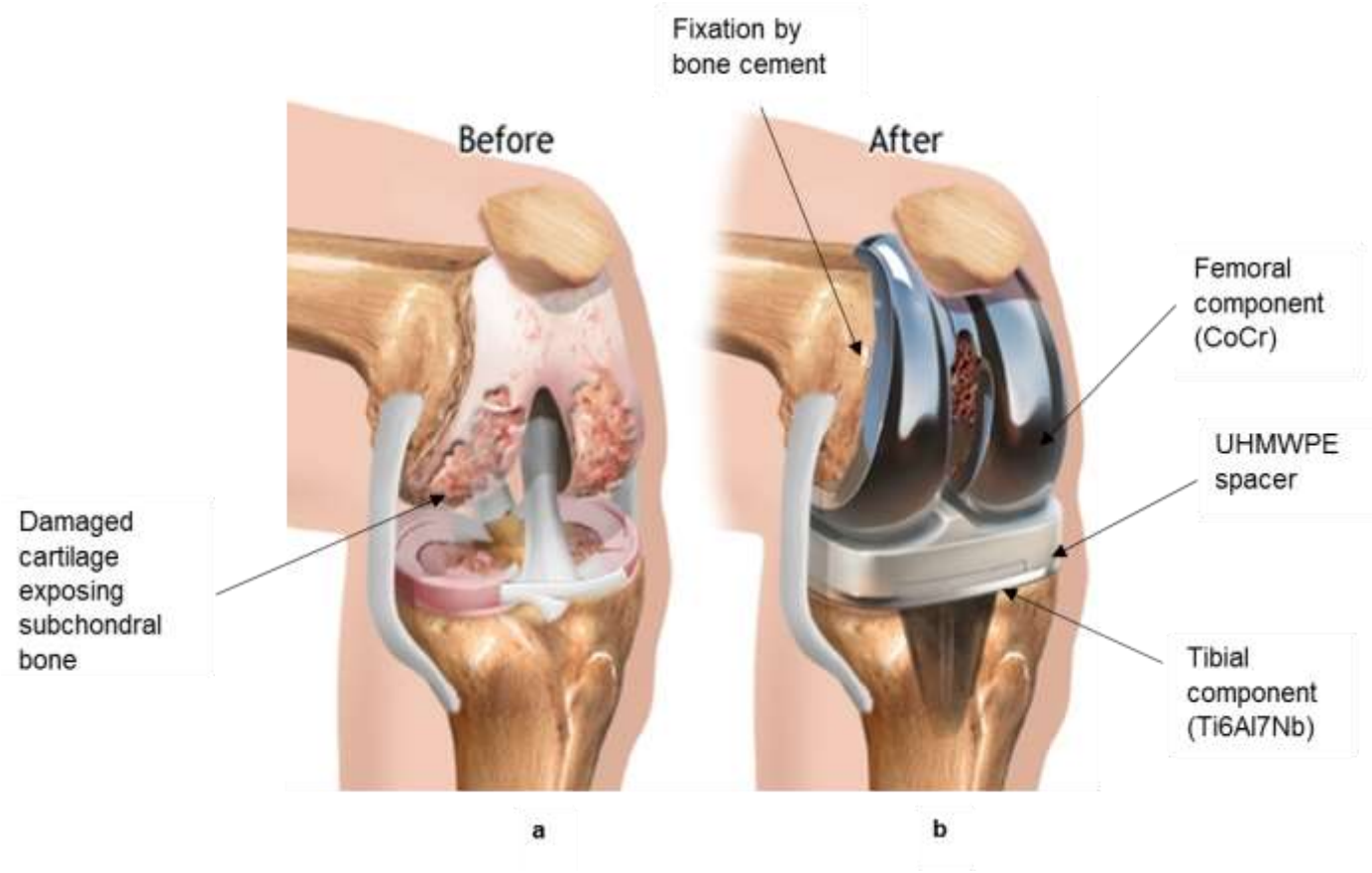

Figure 1.2. A representation of an osteoarthritic knee joint before and after total knee replacement surgery. The impaired knee (a) shows cartilage damage and bone abnormalities and is replaced with an artificial joint implant (b) made of metal and plastic components [7].

1.1.2 Implant associated infections and their causes

Although TJR has proven to be an effective solution to manage osteoarthritis, material-induced infection and foreign body response remain major challenges for implanted medical devices. Implant associated infections (IAI) are severe complications which result in osteomyelitis and have devastating effects on bone and surrounding soft tissue. Fig. 1.3 shows a patient's knee which has become severely inflamed due to an infection after total knee replacement (TKR) surgery. IAI are relatively common and are estimated at 1% for hip replacement surgery and between 1% and 2% after TKR surgery every year [5]. According to data for the United States, the most common cause of revision TKR surgery was infection which accounted for 25.2% of all revision surgeries [6]. Therefore it is clear that IAI affect a large number of TJR surgeries. Moreover, people who suffer with common ailments such as rheumatoid arthritis and diabetes as well as age, malnutrition and obesity tend to be at a higher risk of developing an IAI post-surgery [8]. Further, IAI are associated with substantial patient morbidity and prolonged hospital stays leading to increased financial burden on healthcare systems and patients.

IAI occur when pathogens come in contact with the surface of the implant. Bacteria are the most common pathogen causing IAI. Sources of contamination include airborne bacteria in the hospital environment, bacteria from the patients' skin and from the surgeons' hands and instruments during surgery. Contamination occurs despite preventative measures which are in place such as strict guidelines during

surgery, advanced sterilization techniques and administration of systemic antibiotic prophylaxis to the patient. When bacteria become entrapped on the implant surface or in the patient's body, IAI may occur in the days following surgery.

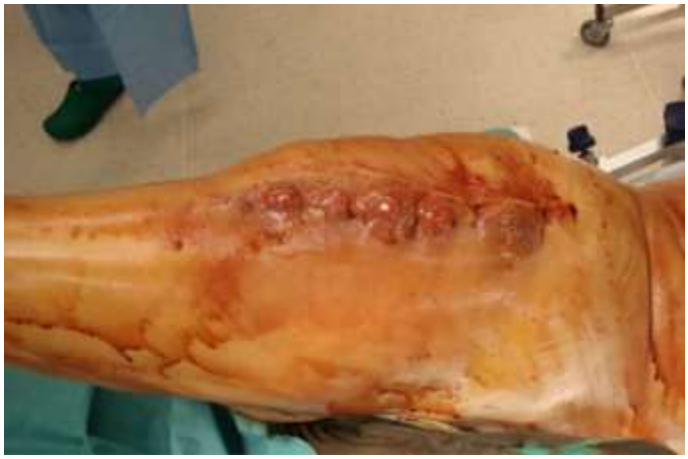

Figure 1.3. An infected knee after total knee replacement surgery showing severe inflammation [5].

Staphylococcus aureus (S. aureus) and *Staphylococcus epidermidis (s. epidermidis) are* gram positive bacterial species which together account for a majority of orthopaedic IAI [9]. A worrisome development in recent years has been the rise of bacterial strains which are resistance to antibiotics. One such strain is Methicillin-resistant Staphylococcus aureus (MRSA), a so called superbug, which is resistant to multiple antibiotics and is also one of the most critical causes of IAI [10]. To make matters worse, bacteria have a tendency to aggregate on implant surfaces *in vivo* and develop into biofilms which are practically resistant to antibiotics. Generally, biofilms can be described as microbial agglomerations embedded in an exopolymeric matrix which survive in an altered metabolic state compared to their surroundings. This unique environment provides protection to the bacteria residing inside the biofilm form the host immune response. Due to these factors, once a biofilm is formed on an implant surface, it is practically impenetrable and resistant to antibiotics. Some antibiotics are even known to induce the formation of a biofilm [11]. Fig. 1.4 illustrates the steps involved in the development of a biofilm. Initially, planktonic bacteria adhere to the implant surface. This is followed by rapid proliferation and secretion of an extracellular exopolymeric matrix which envelops the bacteria. In the next stage maturation of the biofilm occurs and finally single cells detach from the biofilm and move to other areas of the biomaterial and the process repeats.

1.2. Biomaterial strategies to prevent implant associated infections

1.2.1 Antibacterial surfaces

Clinically, in the case of cemented implants, loading the bone cement with antibiotics may be a strategy to reduce or prevent incidence of IAI. However, for cementless implants no suitable strategies to deliver antibacterial agents to the implant surface are in clinical use yet. Since cementless implants have to interact with surrounding bone tissue to achieve stable fixation, the surface properties of the implant are extremely important. Thus a potential antibacterial surface at the bone-implant interface is a strategy which could potentially prevent bacterial infection due to an implant and thereby aid in osseointegration and wound healing.

Such an antibacterial surface would ideally have the ability to preserves host cell interactions as well as stimulate osseointegration while selectively inhibiting the adhesion and survival of bacteria on it or in the

vicinity of the implant. The development of such a surface is one of the major focus areas of research to resolve the problem of IAI. In order to achieve this, one of the popular biomaterial strategies makes use of surfaces which prevent adherence, proliferation and existence of bacteria in the peri-implant region. Some of the approaches to this strategy include use of anti-adhesive materials such as special types of polymer

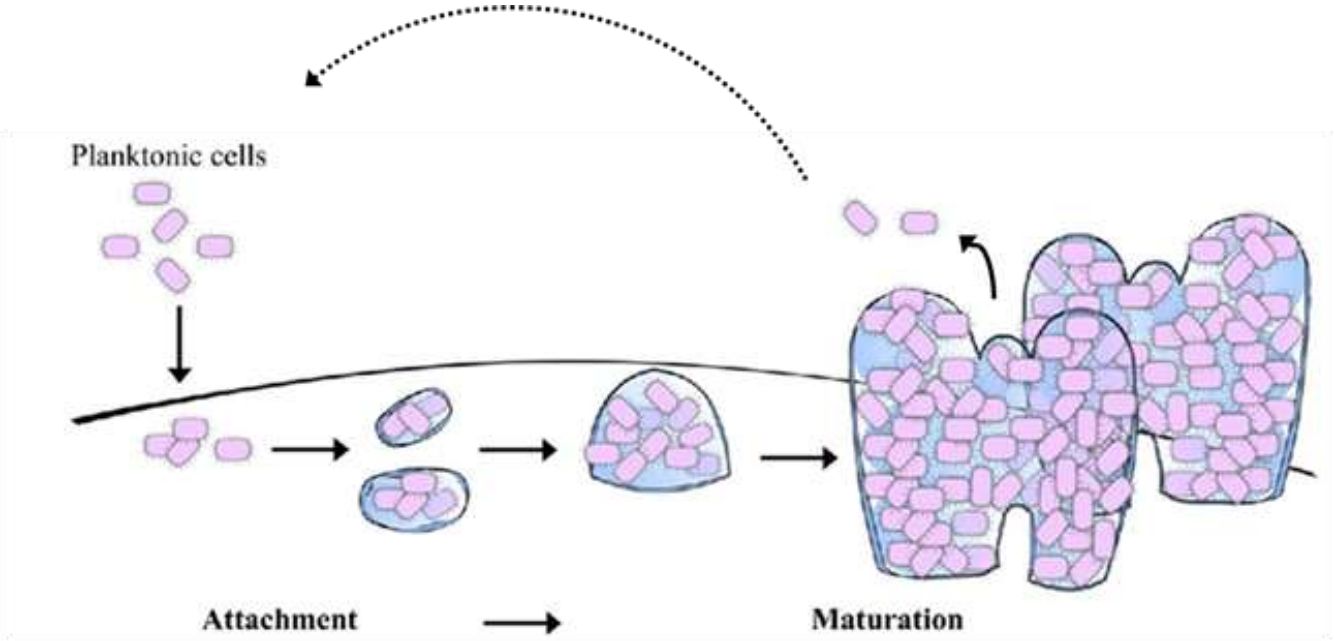

Figure 1.4. Schematic diagram of the main steps involved in the development of a biofilm [12]. Planktonic bacteria get attached to the implant, proliferate and develop into a mature biofilm. Finally planktonic bacteria are released from the biofilm and the cycle repeats.

[13] [14], extremely hydrophobic surfaces or nano-patterned surfaces which discourage bacterial adhesion [15] [16]. This approach is considered a passive strategy because though bacteria are prevented from adhering to the biomaterial surface they are not killed. The bacteria may affect the surrounding host tissue and continue to pose a threat of infection. However, if passive surfaces are functionalized further by combining with bactericidal materials, more effective antibacterial strategies are possible.

To develop an effective antibacterial strategy for cementless implants, it is important to understand the interactions between the bacteria residing on and around the implant surface and the host environment. In 1987, Gristina *et al.* [17] first proposed the theory about a 'race to the surface', wherein both host cells and bacteria compete with each other to reach the implant surface first. Depending on whether host cells or bacteria arrive first to the implant surface, tissue integration or bacterial colonization is established respectively. Obviously, the latter is preferred and the former is detrimental. As previously mentioned, anti-adhesive surfaces are not necessarily bactericidal. Another disadvantage of an anti-adhesive surface is that it also inhibits host cells from adhering at the implant site, preventing osseointegration.

1.2.2 Antibacterial agents

Another strategy which may be more effective than anti-adhesive surfaces makes use of intrinsically antibacterial surfaces which are bactericidal. In this approach, biomaterial surfaces are modified to include antibacterial molecules, ions or particles which are collectively referred to as antibacterial agents. The mode by which antibacterial agents kill bacteria is by their elution from the surface and upon encountering bacteria cause irreversible damage to the bacterial cells ultimately killing them. Also, when bacteria come in

direct contact with the surface containing antibacterial agents they are killed by contact killing. Numerous potential antibacterial agents have been researched. A number of organic materials such as chitosan have been studied for this purpose [19]. Inorganic materials which have been widely studied including silver and titanium di-oxide (TiO_2) and to a lesser extent copper, selenium and zinc to name a few [20] [21]. Antimicrobial peptides, cytokines and certain enzymes which have the ability to interfere with bacteria by cell-signalling are also potential antibacterial agents [18]. Combinations of these materials and or/strategies can results in multi-functional surfaces with enhanced antibacterial activity.

Silver nanoparticles as an inorganic antibacterial agent has been studied extensively due to its well-known antibacterial properties. However silver is cytotoxic and new research has revealed that certain bacteria possess plasmids which confer them with resistance to silver [22]. Copper is also well known for its antibacterial properties dating back several centuries. However relatively little is known about its potential as an antibacterial agent for implant surfaces compared to silver. Copper has some general advantages over silver. Cu is less cytotoxic than Ag, is an essential trace element in living entities and is cheaper than Ag. Therefore it is worth exploring the potential of copper as an antibacterial agent for use in antibacterial surfaces, on its own and possibly in combination with silver.

1.3. Plasma electrolytic oxidation

Various techniques have been used to successfully incorporate metallic nanoparticles into the surface of titanium alloys. Surface enrichment methods such as ion implantation, plasma immersion ion implantation and powder metallurgy incorporate copper nanoparticles directly into the surface of the substrate. Other methods such as magnetron sputtering and sol-gel introduce layers onto the substrate surface which are doped with copper nanoparticles. Plasma electrolytic oxidation (PEO), also called micro-arc oxidation or anodic spark deposition is an electrochemical method which produces a porous oxide layer on the surface of certain metals. It is a suitable method of synthesising copper-bearing surfaces on Ti alloys as it grows and thickens a native passivating TiO_2 layer which spontaneously occurs on the surface of valve metals such as titanium and its alloys. Simultaneously, constituents of the electrolyte become incorporated into the TiO_2 layer. The TiO_2 layer synthesised by PEO is completely integrated with the substrate and provides exceptional mechanical stability and robustness compared to the other surface modification techniques. Moreover the chemistry of the synthesised oxide layer can be tailored during PEO. Additionally, PEO can oxidise very complex surface geometries unlike some of the other synthesis methods and provides a good quality, thick and uniform oxidation layer. The PEO process itself is not as elaborate as other surface modification methods which often require skilled technicians, pre and post treatments of the substrate and use of vacuum chambers and other expensive equipment. PEO can be performed at room temperature with minimal equipment and does not require pre and post-treatment of the substrate being oxidised.

1.4. Aim of the thesis

The aim of the thesis was to produce an antibacterial surface bearing Cu nanoparticles on Ti6Al7Nb biomedical alloy. The phases of the research included the synthesis, surface physico-chemical characterization and *in vitro* evaluation of the antibacterial activity of porous TiO_2 surfaces bearing copper nanoparticles on Ti6Al7Nb. The layout of the research is presented in Fig. 1.5.

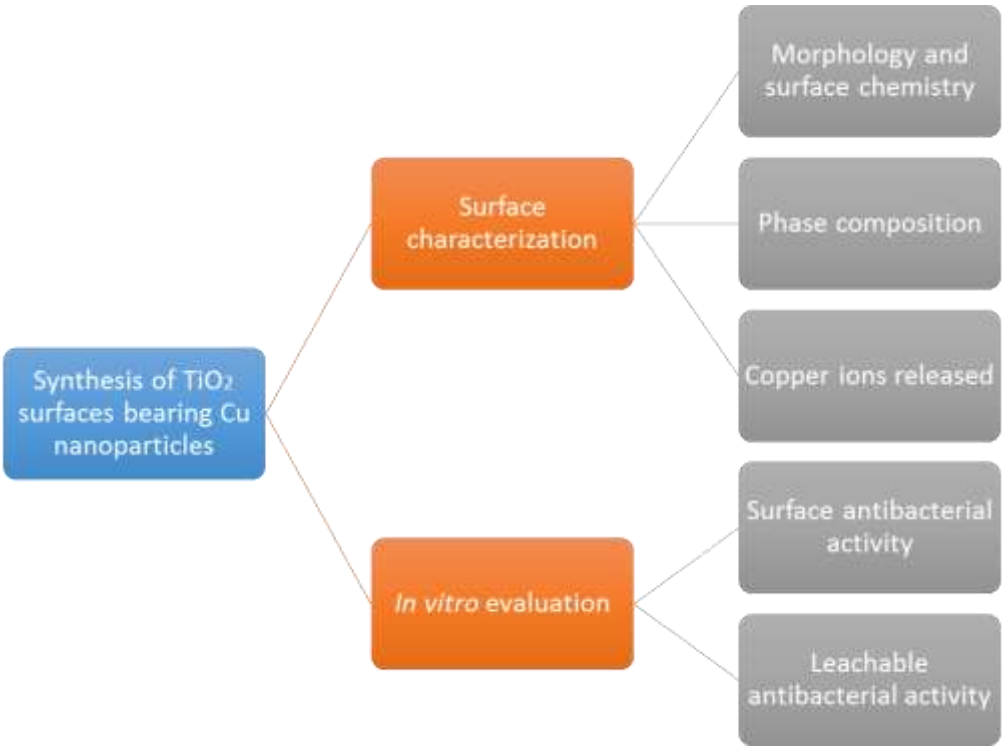

Figure 1.5. Schematic representation of the outline of the research

2 Materials and methods

2.1. Materials

2.1.1 Ti6Al7Nb substrate

2.1.1.1 General

Ti6Al7Nb was first synthesised in Switzerland in 1977. A hip prosthesis made from Ti6Al7Nb was first put to clinical use in 1986. Nowadays it is widely used as a biomedical material for mostly orthopaedic applications. Ti6Al7Nb is an alloy of titanium (Ti) containing 6 percentage by mass Aluminium and 7 percentage by mass Niobium (Nb), hence the nomenclature. This alloy is very similar in its mechanical properties to a versatile Ti alloy Ti6Al4Va which has been popular as a biomedical material for a long time. However, the presence of Vanadium (V) which is cytotoxic, led to V being replaced with Nb based on the principle that the use of only non-toxic elements as implant materials is appropriate [23]. Structurally, Ti6Al7Nb is composed of Ti in both the hexagonal close-packed alpha (α) phase and body-centred cubic beta (β) phase and the phases are stabilized by Nb [24]. It is a highly biocompatible material and has a modulus of elasticity equal to 105 GPa which is similar to that of bone, making it suitable for orthopaedic applications.

2.1.1.2 Preparation of discs

The research was performed on Ti6Al7Nb biomedical alloy (ACNIS International, France) machined from forged bars in the shape of discs. The dimensions of a representative disc were measured using a Vernier callipers and found to have a thickness of 7.9 mm and a diameter of 21.8 mm (Fig. 2.1). The discs had a small threaded hole drilled into each of them with a diameter of 4.5 mm. Based on the measured dimensions, the surface area of the disc was calculated and found to be ~15.9 mm^2.

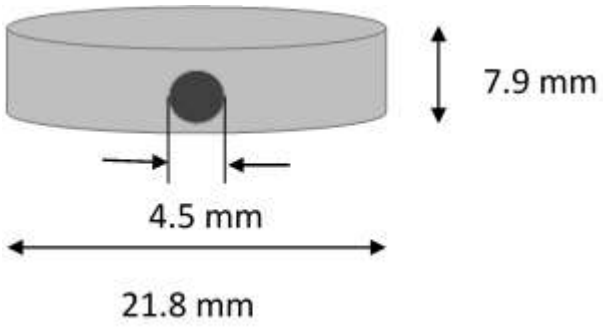

Figure 2.1. Schematic drawing of a sample Ti6Al7Nb disc indicating the value of its diameter, thickness and diameter of threaded hole.

All discs were ground with successive 180, 320, 800 and 1200 SiC abrasive paper (Struers, Denmark). Water acts as a lubricating agent in the grinding process shown in Fig. 2.2. Each disc was ground for 5 minutes with each type of abrasive paper. A grinding technique was adopted which results in a light striation

pattern on the disc surface rather than a smooth mirror finish. After grinding, the samples were thoroughly cleaned with acetone to remove traces of oil by placing the sample in a beaker of acetone and using an ultrasonic bath for 5 minutes. This was followed by cleaning with ethanol and deionized water using the same procedure as that used for acetone. In between each step the sample was dried thoroughly. The samples we kept clean and stored.

Figure 2.2. Ti6Al7Nb sample ground with SiC abrasive paper using water as a lubricant prior to PEO treatment.

2.1.2 Cu nanoparticles

Cu nanoparticles were purchased from SkySpring Nanomaterials. The Cu nanoparticles have a purity of 99.9% and appear as a black nanopowder (Fig. 2.3a). The particles have a spherical morphology with a particle size of 40-60 nanometres (nm) as revealed by transmission electron microscopy (TEM) (Fig. 2.3c). The Cu nanoparticles have a bulk density of 0.19 g/cm^3 and true density of 8.9 g/cm^3[25].

2.1.3 Ag nanoparticles

Ag nanoparticles of 99.5% purity were purchased from Sigma-Aldrich. The Ag nanoparticles appear as a dark grey lustrous powder (Fig. 2.3b) with a spherical morphology and particle size of 7-25 nm in size (Fig. 2.3d) [15] [16].

2.2. PEO process

2.2.1 Equipment

A laboratory scale set-up was customized for the PEO process as shown in Fig. 2.4.The main components are an AC power supply, ACS 1500 (ET Power System Ltd., UK), a Haake V15 thermostatic bath, a computer interfaced with the AC power supply through a data acquisition board (National Instruments SCXI), a double walled glass cylindrical electrolytic cell (Fig. 2.5a) with two electrodes (the counter electrode is made from stainless steel and the anode is a Ti6Al7Nb disc) and a thermocouple that continuously monitors the temperature during the process.

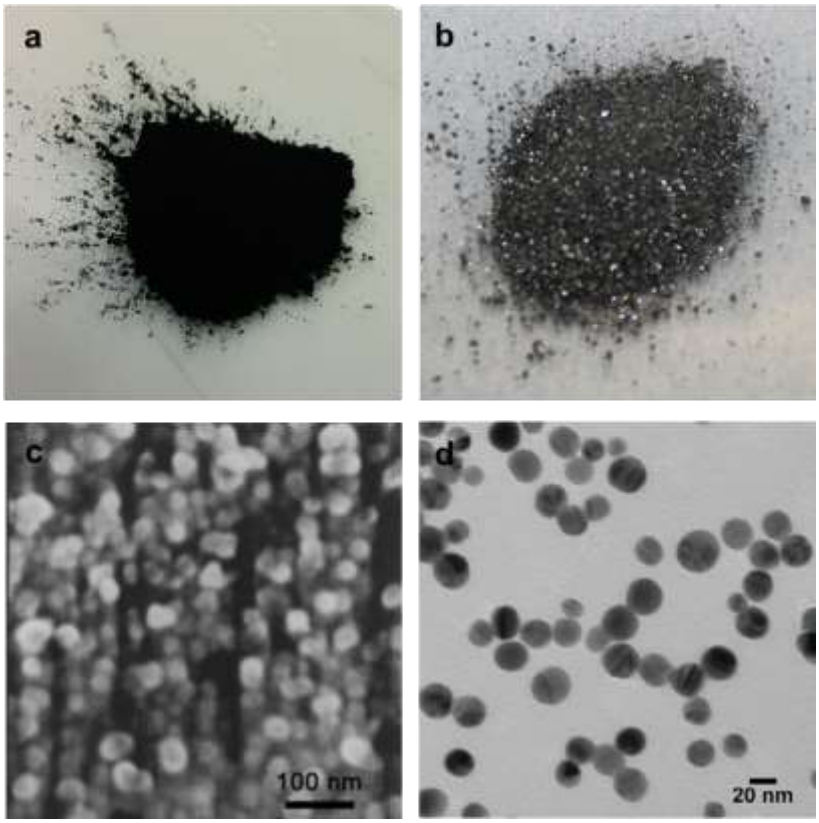

Figure 2.3. General appearance of Cu nanopowder (a) and Ag nanopowder (b). Representative TEM images of Cu nanoparticles of size 40-60 nm (c) and Ag nanoparticles of size 20 nm (d) [25] [26] [27].

2.2.2 Synthesis of Cu and Ag-based surfaces on Ti6Al7Nb discs

2.2.2.1 Electrolyte preparation

An electrolyte was prepared by dissolving 4.2 g/L (0.02M) calcium glycerophosphate (Ca-GP) and 24 g/L (0.15M) calcium acetate (CA) salts in double distilled water. To synthesise TiO_2 surfaces containing Cu or Ag nanoparticles, 3.0 g/L of the respective nanoparticles were dispersed in freshly prepared electrolyte. An ultrasonic bath was used for 5 minutes for a better dispersion of the Cu nanoparticles in the electrolyte. The particle suspension was then stirred for 5 minutes using a magnetic stirrer (700 rpm). The two steps with the ultrasonic bath and magnetic stirrer were repeated. 800mL of the electrolyte was added to the double-walled glass electrolytic cell (Fig. 2.5b) ready for the synthesis of the oxide layers.

2.2.2.2 PEO synthesis

It is worth noting that the following steps are identical for PEO of TiO_2 layers free of Cu nanoparticles on the Ti6Al7Nb discs as well as for CuNP TiO_2 layers. The electrolyte was cooled to 4 - 7°C by circulating a mixture of water and glycerol through the double walls of the cell using the thermostatic bath. A magnetic stirrer at 500 rpm constantly stirred the electrolyte to maintain the particle dispersion. The PEO synthesis was performed under constant current density (galvanostatic mode) of 20 A/dm^2 over a period of 5 minutes. These parameters were selected because they are found to be optimal for the system being used based on earlier experiments [26]. Using the representative total surface area of a disc (measured and calculated in 2.1.1.2), calculations were made and a current of 2.543 A was found to be necessary to maintain the required current density of 20 A/dm^2.

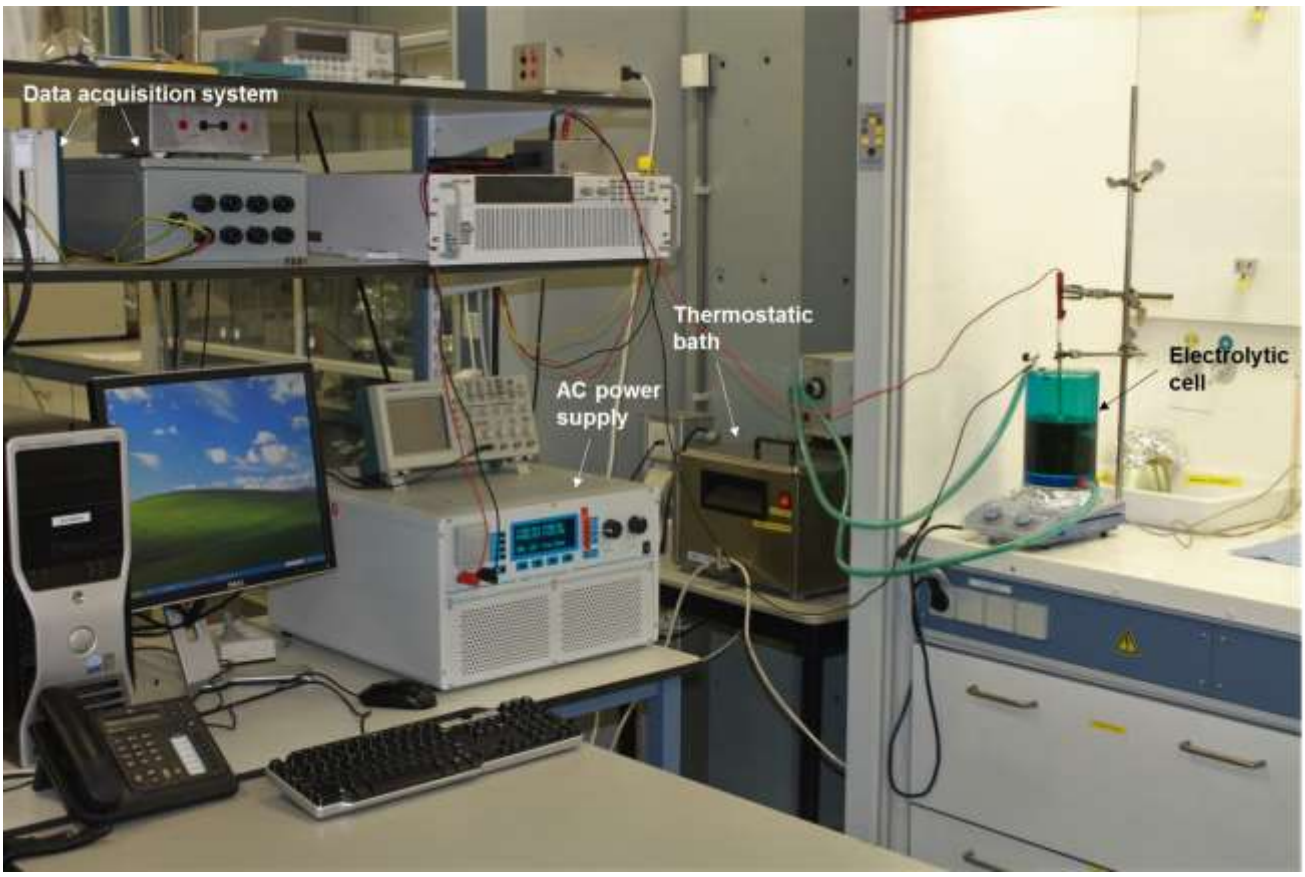

Figure 2.4. Photo of the customized set-up for PEO synthesis

To calibrate the power supply, a dummy sample was fixed to a holder as an anode and the current supplied by means of the AC (50 Hz) power supply was adjusted to 2.534 A using a control knob. Thereafter, a Ti6Al7Nb sample was affixed on the holder by means of the threaded hole machined into it for the purpose. The holder with the sample was suspended in the middle of the electrolytic cell such that the sample was submerged in the electrolyte. Subsequently the electrical connections were made, the power supply was switched on and the oxidation process commenced. During this time, the voltage–time transients were recorded at 1-second intervals using a computer interfaced with the AC power supply through a National Instruments SCXI data acquisition system. The current was switched off after 300 seconds and the synthesis seized. After the synthesis, the samples were washed in running tap water for 5 minutes, ultrasonically cleaned in ethanol, rinsed for a further 5 minutes in deionized water and dried for 1 h at 110°C using a Nabertherm TR60 oven. This process allows the removal of any unattached Cu nanoparticles from the surfaces. The electrolyte constituents and synthesis process parameters are listed in Table 2.1.

Table 2.1. Sample codes, electrolyte constituents and process parameters used.

	Electrolyte constituents			Process parameters				
Sample code	Calcium acetate, g/L	Calcium glycero-phosphate, g/L	Cu nano-particles, g/L	Current density, A/dm^2	Final voltage, V	Oxidation time, minutes	Electrolyte Temperature, °C	
							start	end
PEO	24	4.2	0	20	237±5	5	7±2	29±2
CuNP	24	4.2	3	20	242±4	5	7±2	29±2
AgNP	24	4.2	3	20	236±4	5	7±2	29±2

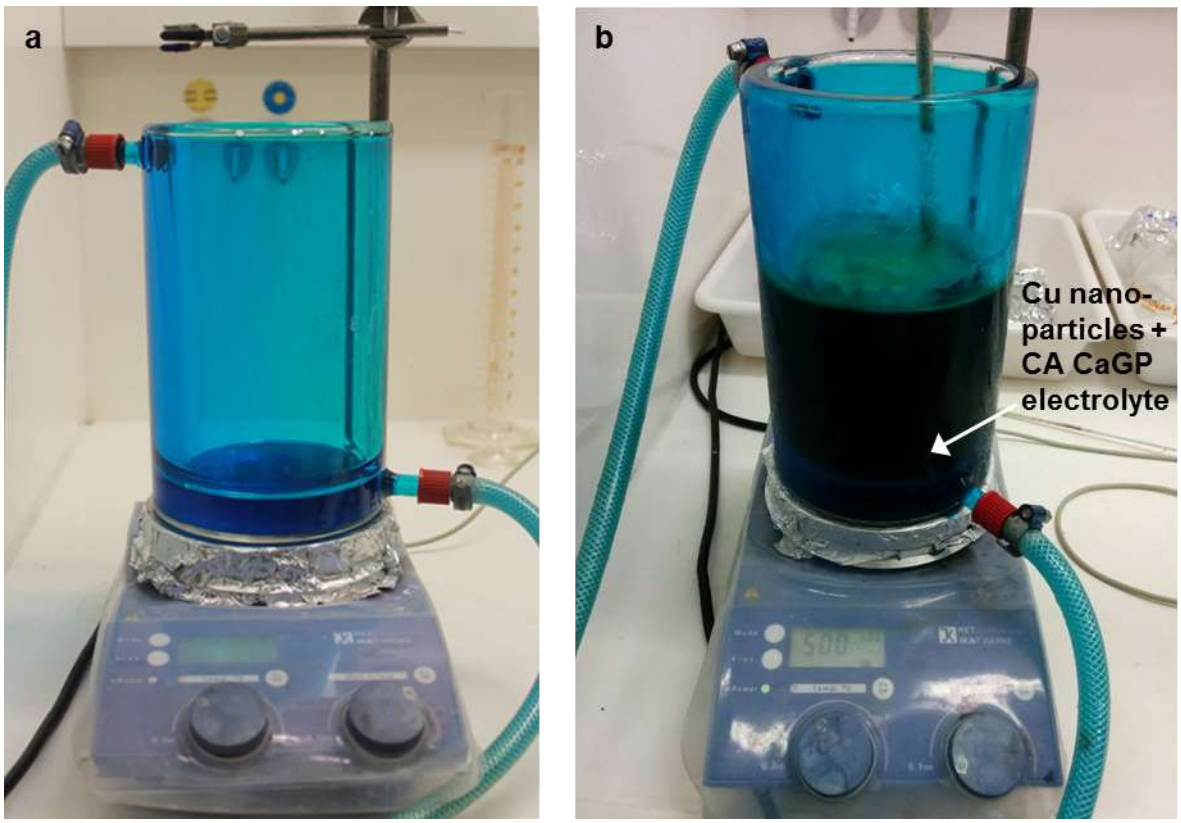

Figure 2.5. The double walled electrolytic cell with coolant circulating through it is used during PEO (a), the cell is placed on a thermocouple to monitor temperature. The electrolytic cell with CA Ca-GP electrolyte and 3.0 g/L Cu nanoparticles dispersed in the electrolyte (b).

2.3. SEM-EDS analysis of the CuNP TiO_2 layers

The Cu-free and CuNP TiO_2 layers synthesised by PEO on the Ti6Al7Nb discs were photographed with a digital camera and their appearance observed with the naked eye. The surface morphology and surface chemistry of the Cu-bearing TiO_2 layers were investigated by scanning electron microscopy (SEM) and energy dispersive X-ray spectroscopy (EDS) analyses on a JSM-IT100LA (JEOL, Tokyo, Japan) microscope. Both secondary and backscattered electrons SEM imaging modes were used. Electron beam energies ranging from 5-20 kV and a working distance of 10 mm were used. Prior to imaging, the samples were cleaned in acetone and 2-isopropanol for 2 minutes each and then sputtered with a uniform carbon layer to ensure a better electrical conductivity.

2.4. XRD analysis of Cu-bearing Ti6lAl7Nb substrate

Quantitative phase analysis of the Ti6Al7Nb alloy, Cu-bearing layers and Cu-free layers was performed by X-ray diffraction (XRD). Initially, a sample disc of each type was fixed in a sample holder with plasticine. The measurements were performed using a Bruker D8 Advance X-ray diffractometer equipped with Bragg-Brentano parafocusing geometry, graphite monochromator and Vantec position sensitive detector using CoKα radiation. The main operating parameters used were a slit divergence of 6M16 V12, scatter screen height of 8 mm, 45 kV and 35 mA with the test sample spinning at 30 rpm. The collected data was evaluated using Bruker software Diffrac.EVA version 4.1.

2.5. ICP-OES analysis of released Cu and Ag ions

An experiment to study the release of Cu^{2+} from the TiO_2 layer were performed in triplicate for the CuNP and AgNP titanium discs. The discs were placed in dark Wheaton bottles containing 30 mL of phosphate-buffered saline (PBS) (Fig. 2.6a) and kept at 37°C under gentle stirring conditions in a water bath for up to 60 days. After the first 6 hours, the discs were transferred to different bottles with fresh PBS (Fig. 2.6b) and the collected liquid was stored in a refrigerator. The samples in the fresh PBS were placed back in the water bath. This process was repeated after 12h, 1 day, 2, 4, 8, 16, 24, 30 and 60 days. All the collected liquid samples were acidified with 5% nitric acid to dissolve the metals in the liquid. Thereafter the liquids were analysed by Inductively Coupled Plasma - Optical Emission Spectrometry (ICP-OES) technique using the PerkinElmer Optima 3000DV instrument.

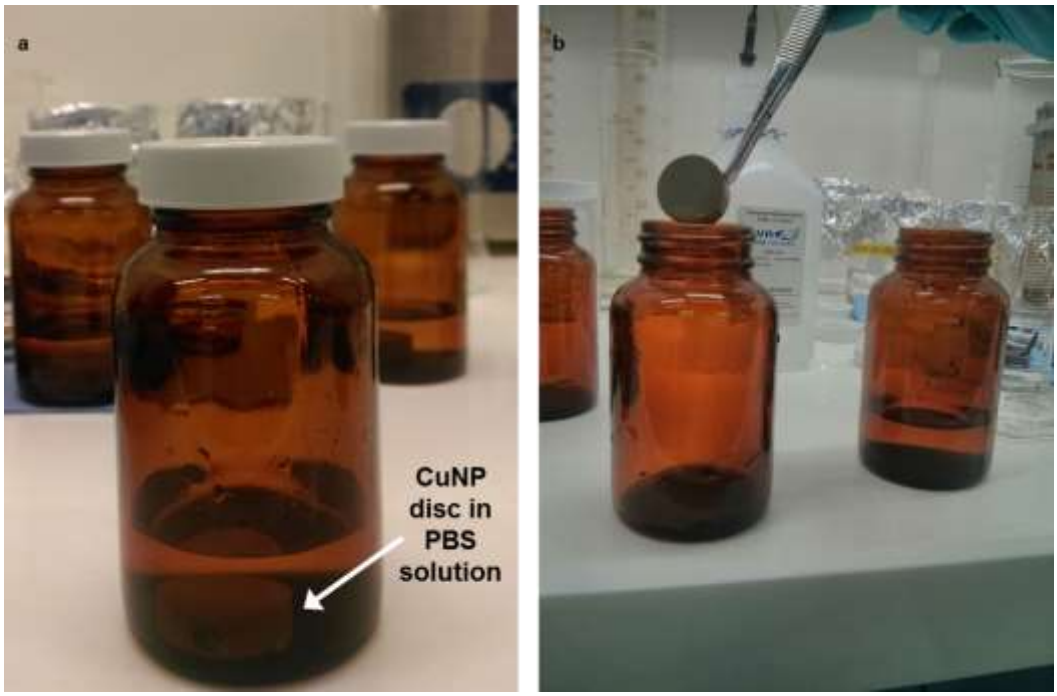

Figure 2.6. CuNP disc submerged in PBS (a) before being placed in a water bath. Collection of leaching liquid at specific time points over a period of 60 days (b).

2.6. *In vitro* evaluation of antibacterial activity

Ti6Al7Nb discs were treated by PEO with the same equipment and by the method described in section 2.1. For an experiment to test the surface antibacterial activity of CuNP TiO_2 layers, 18 samples were prepared. Six samples free of nanoparticles and 6 each with CuNP and AgNP bearing TiO_2 layers.

2.6.1 Direct contact assay

The bactericidal activity of the Cu-bearing TiO_2 layers against bacterial species MRSA and *S. aureus* was evaluated using a modified version of the Japanese Industrial Standard, JIS Z 2801:2000 [26][28].

2.6.1.1. Determination of bacterial concentration

The JIS test is based on utilization of a specific bacterial concentration per surface area. Bacteria are added on the surface of the sample discs and each is covered with a piece of parafilm for even distribution of bacteria on the surface. The discs are then incubated and subsequently sonicated together with the parafilm pieces. Finally, the sonicated fluid is quantitatively cultured to gauge surface bacterial activity.

The diameter of the sample discs used as previously stated is approximately 22 mm (sec. 2.1.1.2). Circular parafilm pieces were prepared such that they are slightly smaller than the discs with a diameter of 20mm (6.28cm^2 in area). Based on the standards set out in the JIS test, an inoculum concentration between 2.5 x 10^5 and 1X10^6 colony forming units (CFU) per mL is recommended. Therefore an inoculum with bacterial concentration 4.05x10^4 CFU of *S. aureus* and 3.75x10^4 CFU of MRSA in 60 µL for each disc was prepared, which is equivalent to 1.16 x10^6 CFU/mL which is within the recommended range. A volume of 60 µL was chosen for the inoculum because it was sufficient to be distributed over the disc surface without spillage.

2.6.1.2. Preparation of standard inoculum

Fresh liquid cultures of strains AMC201 (MRSA) and RN4220 (*S. aureus*) were prepared by adding 1-5 colonies of each bacterial strain to 20mL Bacto Tryptic Soy Broth (TSB) (Brunschwig Chemie, The Netherlands) in a 100mL flask. The surroundings and flask were kept sterile by working in the vicinity of a Bunsen burner flame which creates an updraft and moves contaminants away from the work area. The cultures were incubated at 37°C under rotation for about 2 hours. Then, 1 .5 mL of each culture was transferred to Eppendorf tubes and centrifuged in a table top centrifuge at 4000 rpm (~3500 x g) for 10 minutes at room temperature. After centrifugation, the supernatant was removed and half a volume (1mL) of 10 mM sodium phosphate buffer, pH 7.0 and 1% TSB (PT) were added and the bacteria re-suspended. This washing step is necessary to remove the growth medium of the liquid cultures.

In a marked 1 cm cuvette, 100 µL of the bacterial suspension was added to 900 µL PBS (1:10 dilution). The optical density (absorbance) at 620 nm (OD620) was measured. The OD_{620} of AMC201 was found to be 3.72 and that of RN4220 was 6.2 after correcting for dilution with PBS. 9.35µL of the AMC201 suspension and 5.6µL of the RN4220 suspension were each subsequently diluted with 10 mL PBS and 1%TSB to an optical density (OD_{620}) of 0.00348 corresponding to 1.16X10^6 CFU/ mL which is the standard bacterial concentration we need.

2.6.1.3. Validation of standard inoculum

It is necessary to verify the ratio between the OD and number of CFU per mL for each bacterial strain since this ratio may be influenced by the growth phase of the bacteria. To do this, both the cultures which were diluted to an OD_{620} of 0.00348, were diluted in a microtiter plate by serial 4-fold dilution (add 10 µL of culture to 90 µL PBS). The dilution is done until there is an estimated 1 CFU per 10 µL to spot on a blood agar plate. Subsequently, 4 aliquots of 10 µL each of the 4 dilutions were pipetted (using a multichannel pipette) onto a blood agar plate and incubated overnight at 37°C. The next day, the colonies in the highest countable dilution (which was found to be 10^{-3}) were counted. Table 2.2 lists the number of CFU in the 10^{-3} row of the four spots for each bacterial species.

Table 2.2. Number of CFU in each spot of the 10^{-3} dilution of AMC201 and RN4220

Inoculum strain	Number of CFU in each spot of the 10^{-3} dilution				Average (CFU/10 µL)
	Spot 1	Spot 2	Spot 3	Spot 4	
AMC201	3	9	9	6	6.75
RN4220	4	7	9	5	6.25

Based on the colonies counted, the number of CFU/mL in the original suspensions were calculated as follows:

Inoculum per mL is calculated as:

For AMC201,

6.75 /10 µL in 10^{-3} dilution = 6.75×10^5 CFU/mL (~1.16×10^6 CFU/mL)

For RN4220,

6.75 /10 µL in 10^{-3} dilution = 6.25×10^5 CFU/mL (~1.16×10^6 CFU/mL)

Therefore the growth phase has not influenced much the ratio between the OD and number of CFU per mL i.e. the bacterial concentration estimated based on the OD value still holds good even after culturing the bacteria.

2.6.1.4. Quantitative bactericidal activity assay

PEO, CuNP and AgNP titanium discs were prepared in triplicate for evaluating their antibacterial activity against MRSA and *S. aureus*. The discs were placed in a petri dishes and 60 µL of the bacterial inoculum containing 4.05 x 10^4 CFU of *S. aureus* was carefully pipetted onto the middle of each disc (3 discs each of CuNP, AgNP and PEO). Similarly, 60 µL of the bacterial inoculum containing 3.75 x 10^4 CFU of MRSA was pipetted onto the middle of each disc (3 discs each of CuNP, AgNP and PEO). The parafilm pieces were carefully placed over the inoculum droplet on each disc and flask caps filled with water were placed in each petri dish to provide moisture. (Figs. 2.7 and 2.8). All petri dishes were placed in a box and were incubated at 37°C for 24 hours in a humid atmosphere. After incubation, each disc along with the corresponding parafilm was placed in flasks containing 5 mL PBS (Fig. 2.9a) and sonicated for 5 minutes and then vortexed for 15 seconds to dislodge adherent bacteria. This step does not have an effect on bacterial viability. Four 10-fold (10^{-1} to 10^{-4}) serial dilutions were made in a 96 well ELISA microtiter plate (Fig. 2.9b).

Subsequently, four 10 µL aliquots of the 4 dilutions were pipetted onto blood agar plates (Fig. 2.9c). The blood agar plates were incubated at 37°C for 24 hours and bacterial colonies counted the next day. To improve the detection limit of the assay, the left over sonicated liquid from the CuNP and AgNP titanium discs was centrifuged leaving behind pellets containing leftover bacteria and any traces left of Cu and Ag nanoparticles respectively. The supernatant was pipetted out leaving behind the pellets in ~200 µL volumes which were plated in total on blood agar plates (Fig. 2.10). The plates were incubated overnight at 37°C.The sample size for this experiment is $n \geq 3$.

2.6.1.5. Statistical analysis

The direct contact assays were performed in triplicate and data was expressed as means ± standard deviations. IBM SPSS Version 24 software package was used to perform that statistical analysis. A two-way ANOVA combined with a Tukey post hoc test was utilized to determine the level of significance. In general, $p < 0.05$ was regarded to be significant and $p < 0.01$ was considered highly significant.

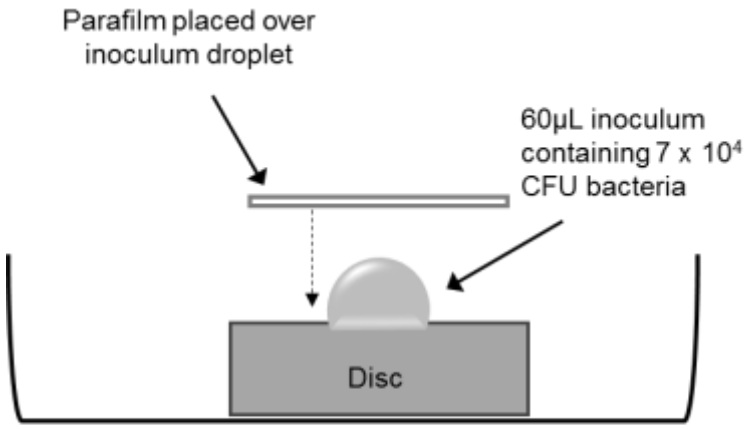

a) The parafilm is placed over the inoculum such that the droplet spreads evenly and bacteria contact the surface of the titanium sample

Figure 2.7.Schematic diagram of the direct contact assay to investigate the antibacterial activity of the Cu and Ag bearing layers. As the parafilm has a diameter smaller than that that of the disc, it helps the inoculum droplet to spread uniformly over the disc surface.

Figure 2.8. CuNP discs in triplicate inoculated with *S. aureus* and covered with parafilm and placed in a petri dish are shown here before they were incubated for 24 hours.

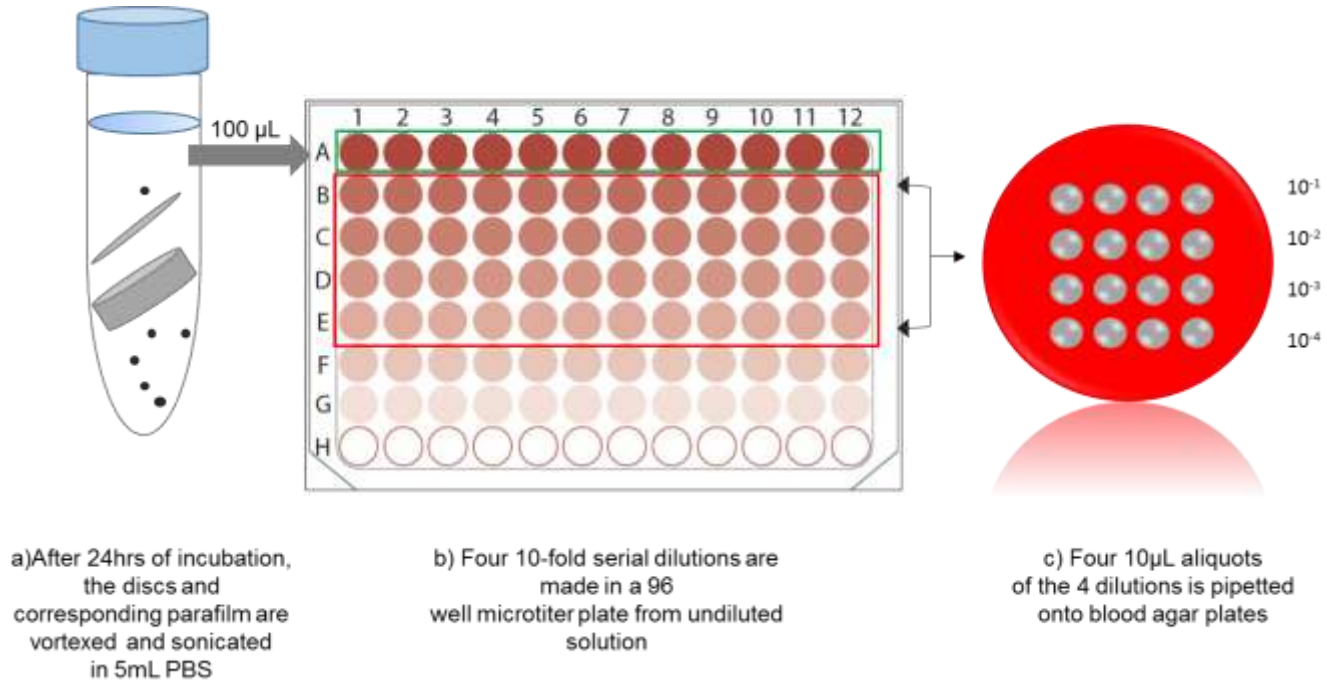

Figure 2.9.Experimental steps to quantify antibacterial activity of the discs against *S. aureus* and MRSA.

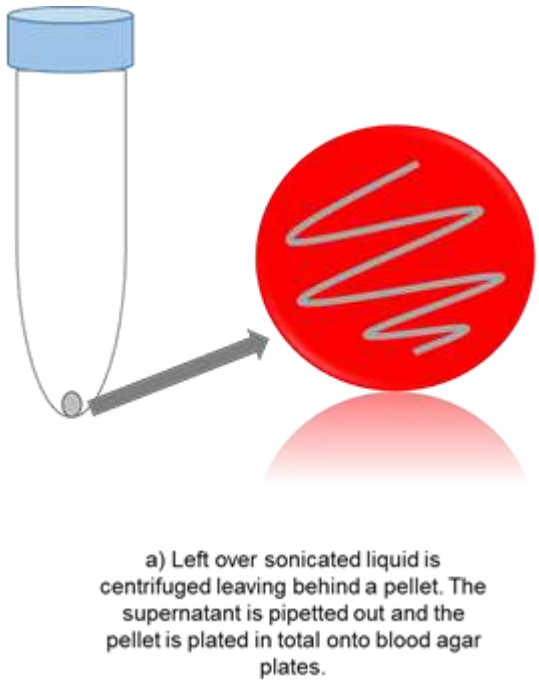

Figure 2.10.To improve the detection limit of the assay, left over pellets of the sonicated liquid of both *S. aureus* and MRSA were plated in whole on blood agar.

2.6.2 Agar diffusion assay

The agar diffusion test is used to evaluate diffused or leached and possibly surface antimicrobial activity of materials. This assay is suitable for testing the antibacterial activity of small materials which are placed on top of bacteria containing agar. The standard assay has been modified to adapt to the size and shape of the titanium discs. One disc each of CuNP, AgNP and PEO were tested. The AgNP disc served as a positive control and the PEO disc served as a negative control.

To prepare the agar, 5 mL of TSB was taken in a 100 mL flask and 1% agarose type 1 (low electroendosmosis (EEO)) which allows easy diffusion of bacteria was added in the flask. The mixture was boiled in a microwave carefully by swirling the flask every few seconds to avoid spillage of the mixture. The mixture was then placed in a water bath at 45°C. After cooling to 45°C, the flask was taken out of the water bath ready for bacteria to be added.

An inoculum of bacterial concentration $4x10^9$ CFU per mL of *S. aureus* strain RN4220 was prepared and 15µL of the inoculum was added to 1.5 mL of warm agar. Therefore, 250 µL of the agar and bacteria mixture had an end concentration of $1x10^7$ CFU. Three microscope slides were pre-warmed and 250 µL agar bacteria mixture was pipetted onto each slide (Fig. 2.11a). The slides were kept warm during the procedure to preserve the agar bacteria mixture and to prevent bacteria from being killed. Large coverslips (24 x 50 mm) were carefully placed over each slide. After a few minutes the agar had solidified and the coverslip were removed. Each titanium disc being tested was carefully placed on a microscope slide with the agar bacteria mixture (Fig. 2.11b). The slides were then placed in covered plastic dished and incubated in a humid atmosphere overnight.

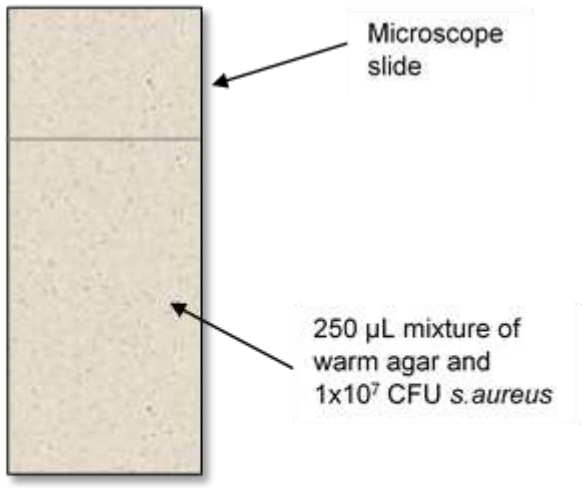

a) Warm agar mixture containing bacteria pipetted onto 3 pre-warmed microscope slides, covered with cover slips and left to solidify

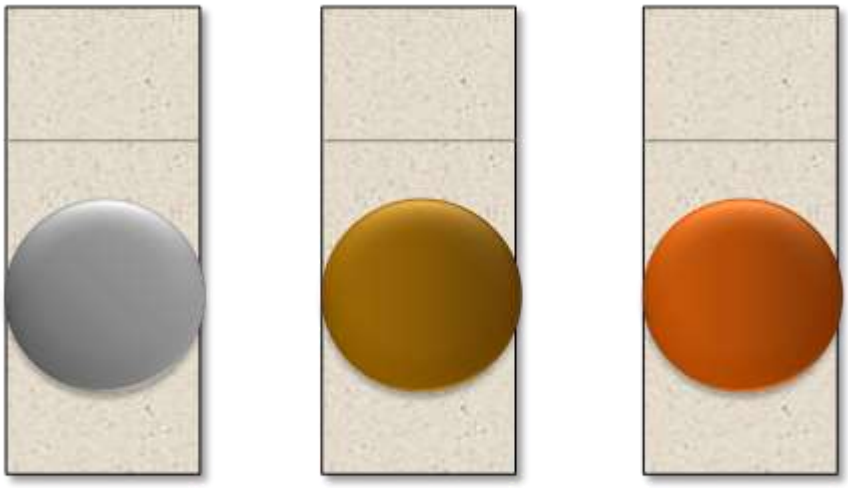

b) After the agar had solidified, the coverslips were removed and one each of PEO (negative control), CuNP and AgNP (positive control) discs were placed on each slide and incubated for 24 hours in a humid environment

Figure 2.11. Experimental steps involved in an agar diffusion assay to investigate leachable antibacterial activity of Cu-bearing layers.

3 Results

3.1. Synthesis of Cu-based TiO_2 layers on Ti6Al7Nb alloy substrate

The Ti6Al7Nb disc acted as an anode and was immersed in the aqueous electrolyte. A constant current density was applied between the anode and a counter electrode over a period of 300 seconds. The changes in the voltage–time transients during oxidation of Ti6Al7Nb discs in i) Cu-free electrolyte and ii) electrolyte with Cu nanoparticles was recorded (Fig. 3.1). It is clear from the graph in Fig. 3.1 that the presence of CuNP does not significantly affect the changes in voltage.

Plasma enhanced electrochemical, thermal and diffusion processes occur during PEO giving rise to modification of titanium disc surface [29]. Oxidation reactions at the anode and reduction reactions at the counter electrode in combination with field-driven ion diffusion lead to the formation of a TiO_2 layer on the Ti6Al7Nb surface. The native TiO_2 film occurring on the Ti6Al7Nb alloy is around 3-7 nm thick and is resistant to the flow of current. The voltage between the electrolyte and the titanium substrate in the cell occurs across the resistance of the oxide layer. In accordance with Ohm's law, as the resistance of the growing oxide layer increases, the corresponding voltage also increases proportionally since current density is maintained constant in the cell. Therefore as observed from Fig.3.1, the initial increase in voltage is sharp and linear corresponding to growth of an amorphous anodic oxide film. A few seconds after the oxidation process is underway, an inflection in the curve followed by a lower rate of voltage increase corresponds to breakdown voltage leading to a decrease in the resistance of the oxide layer and dielectric breakdown. Due to the continuing current density maintained inside the cell, spark discharges called micro-arcs are observed over the disc surface (Fig. 3.2). Since they rapidly develop and extinguish within fractions of a second, the discharges do not heat up the metal substrate much. However, the temperature inside the discharge channels can reach as high as 10^4 K giving rise to plasma thermochemical interactions between the Ti discs and the electrolyte [29]. As the discharges continue, fresh portions of electrolyte reach the bare metal surface. These interactions result in the formation of complex surface compounds composed of oxides of the substrate and also incorporate constituents of the electrolyte. These processes continue as long as the voltage is sufficient for new breakdowns to occur and discharge channels to perforate the thickening oxide layer.

The characteristic breakdown potential for Ti6Al7Nb in the CA and Ca-GP electrolyte was found to be at around 111 V in the presence of a 20 A/dm^2 current density. The overall reactions at the anode and cathode (counter electrode) leading to formation of an oxide layer and incorporation of Cu nanoparticles in the layer can be written as follows [26]:

At anode:

$$Ti^{2+} + 2O^{2-} \rightarrow TiO_2 + 2e^-$$

At cathode:

$$2H_2O \rightarrow 2O^{2-} + 4H^+ \rightarrow H_2\uparrow$$

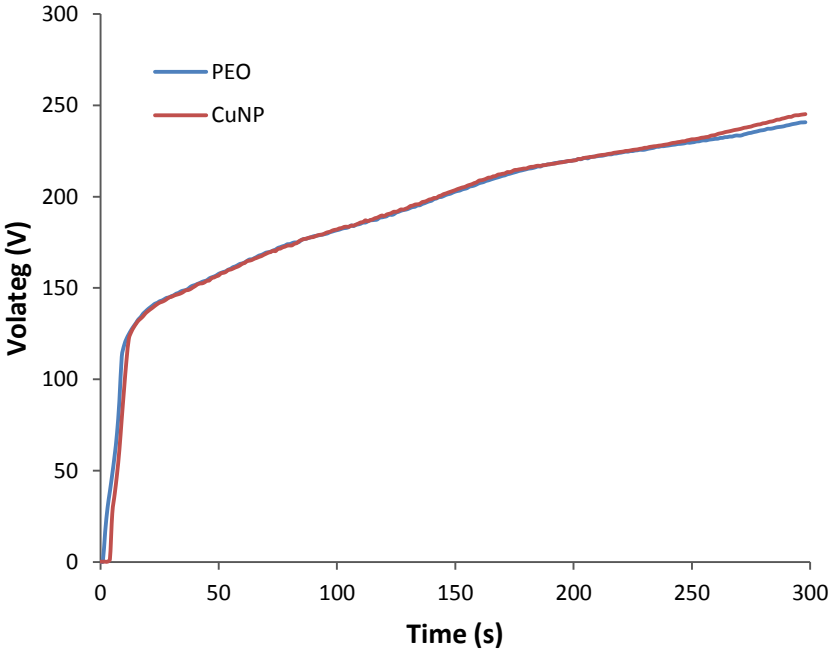

Figure 3.1. Typical profile of the voltage-time transients recorded during PEO treatment of Ti6Al7Nb discs in Ca-GP electrolyte i) Cu-free (PEO) and with ii) Cu nanoparticles (CuNP) added in the electrolyte.

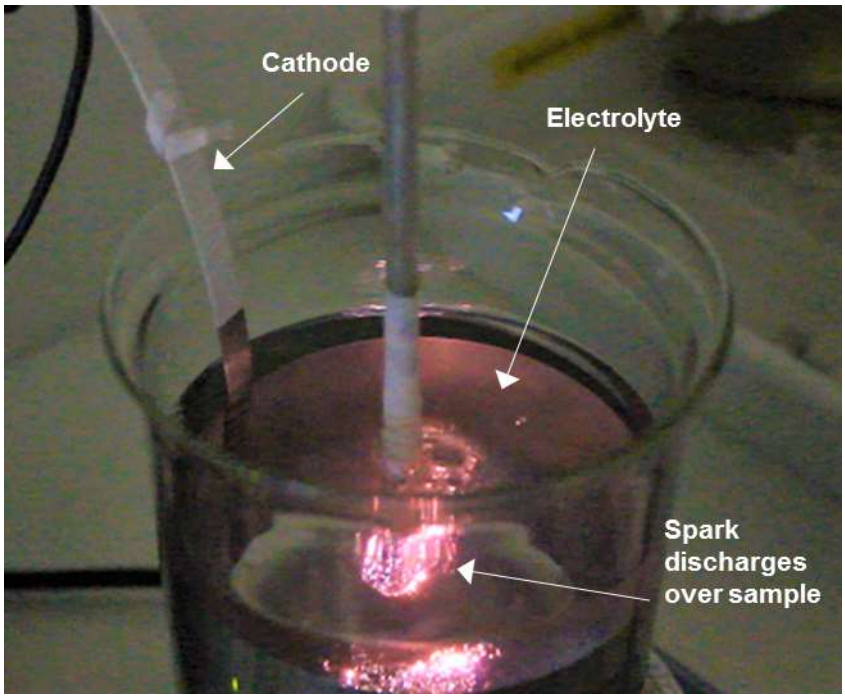

Figure 3.2. Numerous spark discharges generated across the surface of the Ti6Al7Nb disc following dielectric breakdown during PEO, leading to the formation of discharge channels on the disc surface.

3.2. Surface morphology and chemistry of CuNP TiO_2 layers

3.2.1 Macroscopic observation

Photographs of an untreated Ti6Al7Nb disc, Cu-free PEO disc, CuNP disc and AgNP disc (prepared for use as a positive control for experiments performed) are shown in Fig. 3.3. The untreated Ti6Al7Nb discs have a reflective appearance typical of metals. After PEO, the Ti6Al7Nb discs changed in appearance to a grey colour with a matt ceramic finish. The CuNP discs differ from the PEO discs in appearance as they are light brown in colour with a slightly mottled appearance. The light brown colour is attributed to the Cu content of the doped surface which have been incorporated into the surface from the electrolyte during the PEO synthesis. The AgNP discs have a reddish brown mottled appearance and differ in colour from the CuNP discs due to the presence of Ag nanoparticles.

3.2.2 Surface morphology

The oxidised discs were examined after PEO by SEM (Fig. 3.4 and Fig. 3.5). The PEO synthesis altered the surface significantly giving rise to a thick porous oxide layer uniformly distributed over the entire surface of the discs. Fig. 3.4 (a-d) shows SEM images taken at various magnification settings in secondary electron mode (SEM-SED) and reveal numerous microscopic pores varying in size from a few nm up to 10µm on the disc surfaces. The pores are well defined, distinct from each other and interconnected. The pore structures are a consequence of the intensive plasma discharge channels occurring during PEO synthesis. It is through these discharge channels that electrolytic constituents reached the surface of the titanium substrate and became incorporated in the growing oxide layer. Upon cooling, the discharge channels solidified to became porous structures. Additionally, micro cracks are observed on the oxidised surfaces formed by the release of stress which is generated during the PEO synthesis.

SEM images of the discs oxidised by PEO were also taken in backscattered electron mode (SEM-BSE) at different magnifications Fig. 3.5 (a-c). Elements with high atomic number such as Cu, backscatter electrons more strongly than elements of low atomic number such as Ti, Oxygen (O_2), Calcium (Ca) or Phosporus (P) which are also estimated to be present. Thus the presence of Cu is revealed as bright spots in the images due to higher backscattering of electrons. The circled areas in Fig. 3.5 (a and c) highlight the contrast between areas with different chemical compositions and the bright spots reveal the presence of Cu nanoparticles.

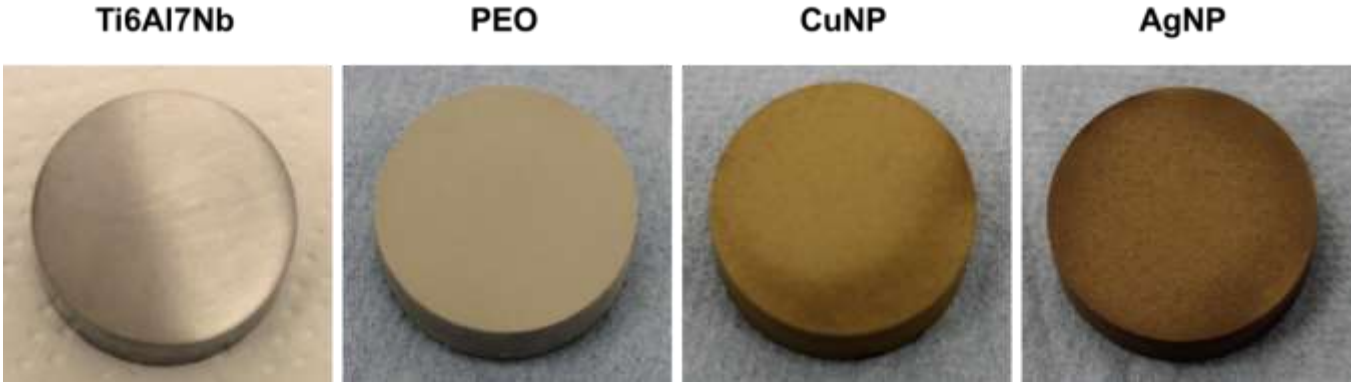

Figure 3.3. Physical appearance of the Ti6Al7Nb disc before PEO and after PEO along with PEO treated discs containing Cu and Ag nanoparticles, respectively.

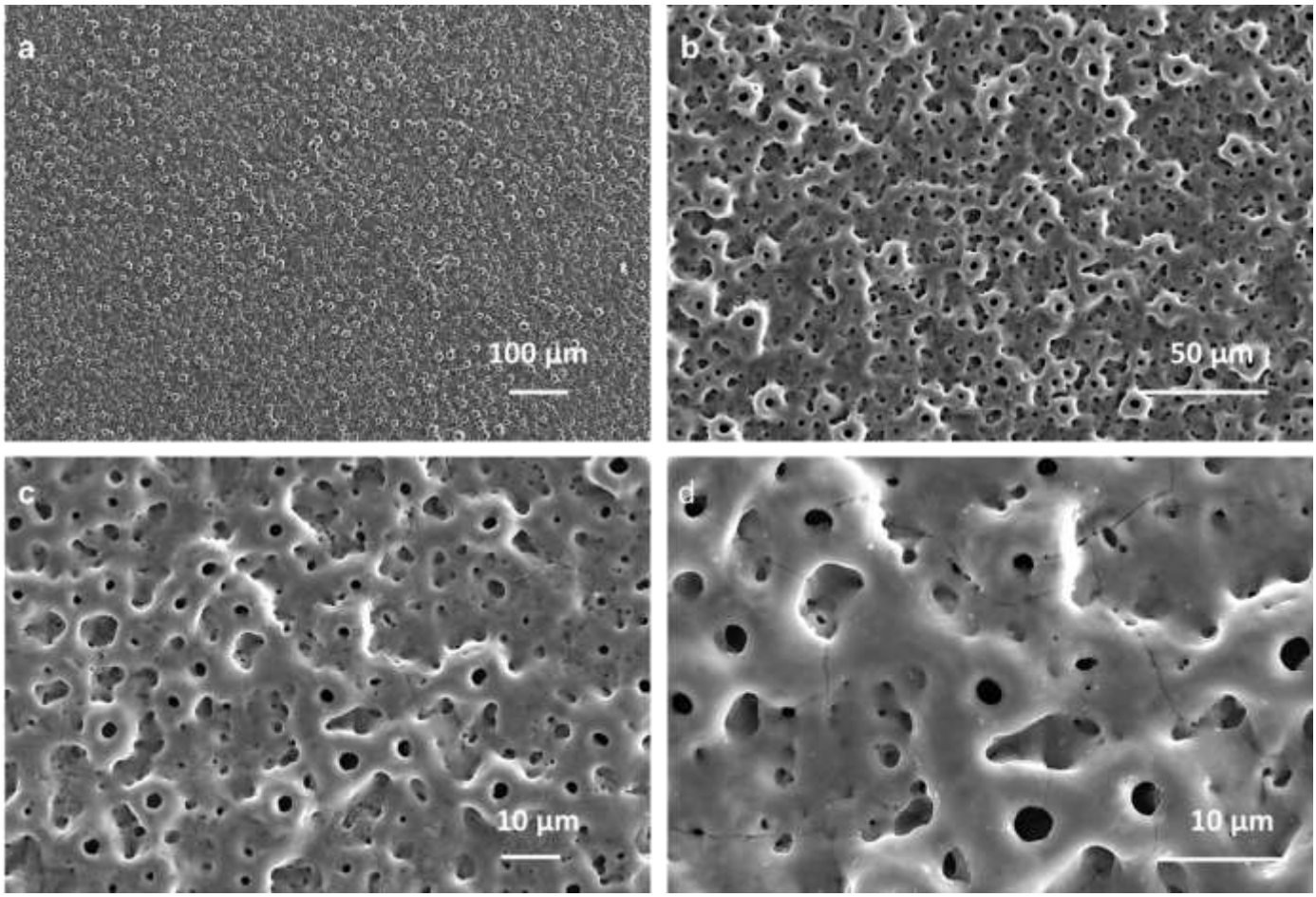

Figure 3.4. The porous surface morphology of Cu-bearing TiO_2 layers magnified 100x (a), 2000x (b) and (c) and 10,000x (d) as revealed by SEM in secondary electron mode.

3.2.3 Chemical composition

The CuNP discs were examined further to identity the particles revealed in the SEM images. The SEM was equipped with an EDS detector and various spots on the disc surfaces were analysed. EDS analysis is frequently used for identification of elements present in a material. The interaction of X-ray excitations with a material give rise to the emission of an electromagnetic spectrum which is unique to each element. Thus, by observing the characteristic peaks of an EDS spectra for a specific area on the TiO_2 layers, the elements present can be identified. Fig. 3.6 is an SEM image of the CuNP TiO_2 surface and the corresponding EDS spectra of the sites analysed. At a spot “a” on the surface which does not have any particles on it, the presence of Ca and P reveals that constituents of the electrolyte had been incorporated into the surface in addition to the elements present in the substrate (Ti, O, Al, and Nb). The EDS spectra at two spots “b” and “c” where particles appear to be present on the surface, clearly indicated the presence of Cu in addition to the other elements already stated which are also present.

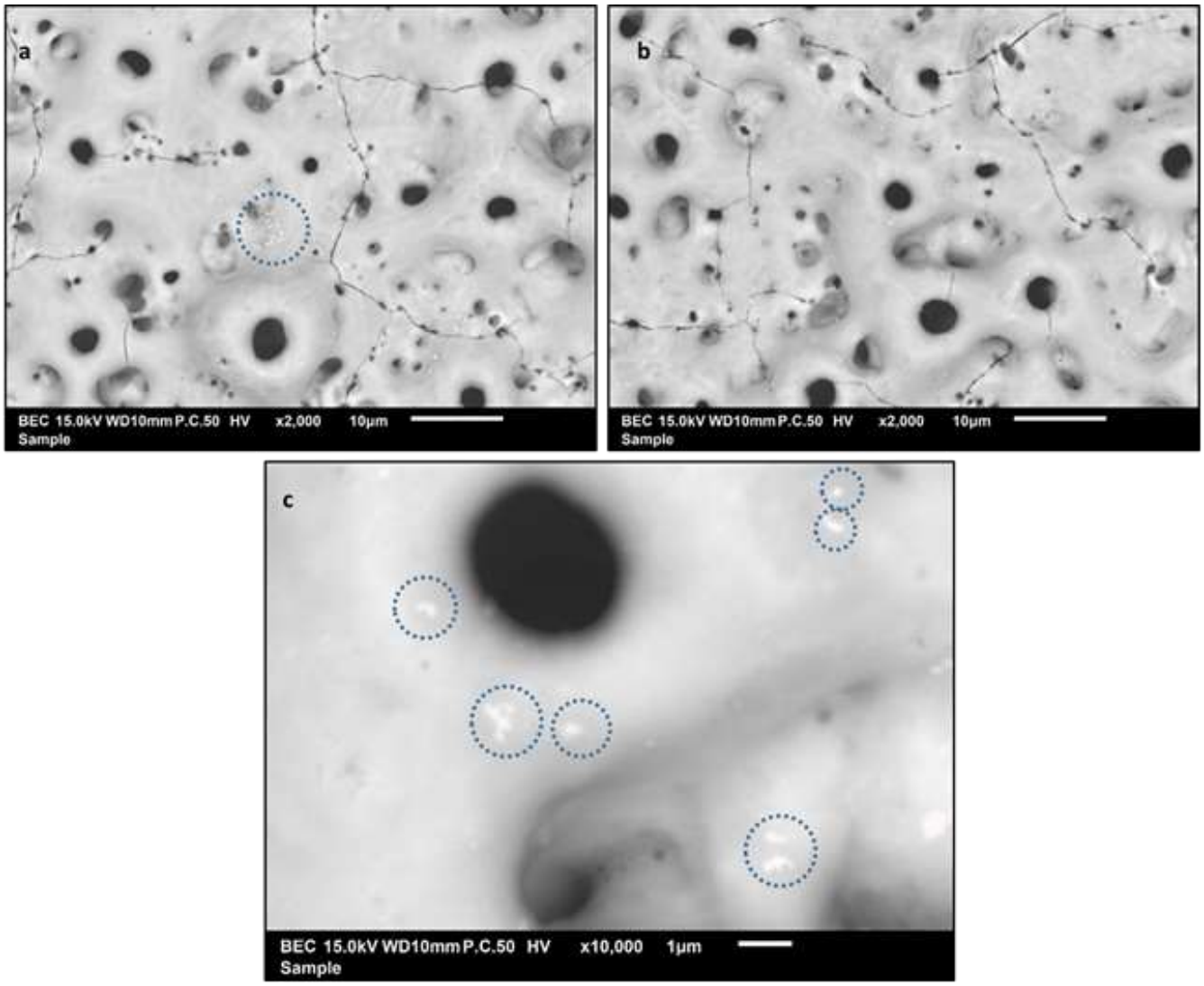

Figure 3.5. The porous surface morphology of Cu-bearing TiO_2 layers magnified 2000x (a) and (b) and 10,000x (c) as revealed by SEM in backscattered electron mode. The light 'spots' highlighted in (a) and (c) indicate the presence of Cu.

3.3. Phase composition of CuNP TiO_2 layers

Fig. 3.7 presents the XRD patterns of the Ti6Al7Nb alloy and the surfaces prepared by PEO in the CA Ca-GP electrolyte with and without added Cu nanoparticles. The main TiO_2 phases present within the oxidized samples were rutile and anatase. The titanium peaks which appeared in the XRD patterns across all PEO treated samples and in the Ti6Al7Nb sample is assumed to belong to the Ti phase present in the Ti6Al7Nb substrate. As mentioned in the introduction, Ti6Al7Nb alloy comprises a mixture of alpha and beta phases (not shown). The XRD patterns of Cu-bearing surfaces did not reveal any Cu or Cu-containing phases. This may be due to the low concentration of Cu incorporated into the porous layers, which is possibly below the detection limit of the XRD analysis.

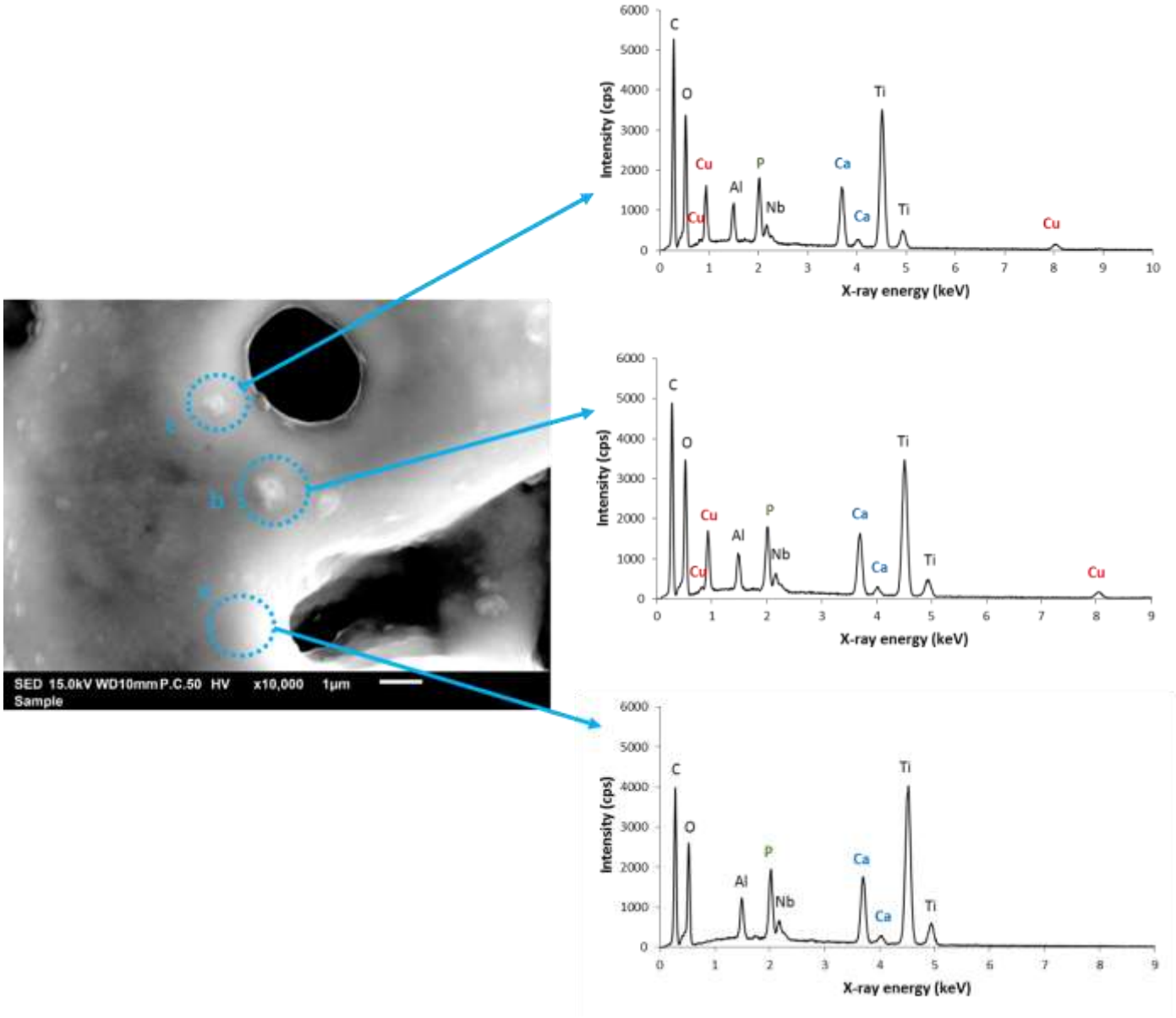

Figure 3.6. An SEM image of a Cu-bearing TiO_2 layer with the corresponding EDS spectra. The EDS chart for spot a revealed the presence of O, Al, P, Nb, Ca and Ti. The EDS chart for spots b and c reveal the presence of Cu in addition to the other elements.

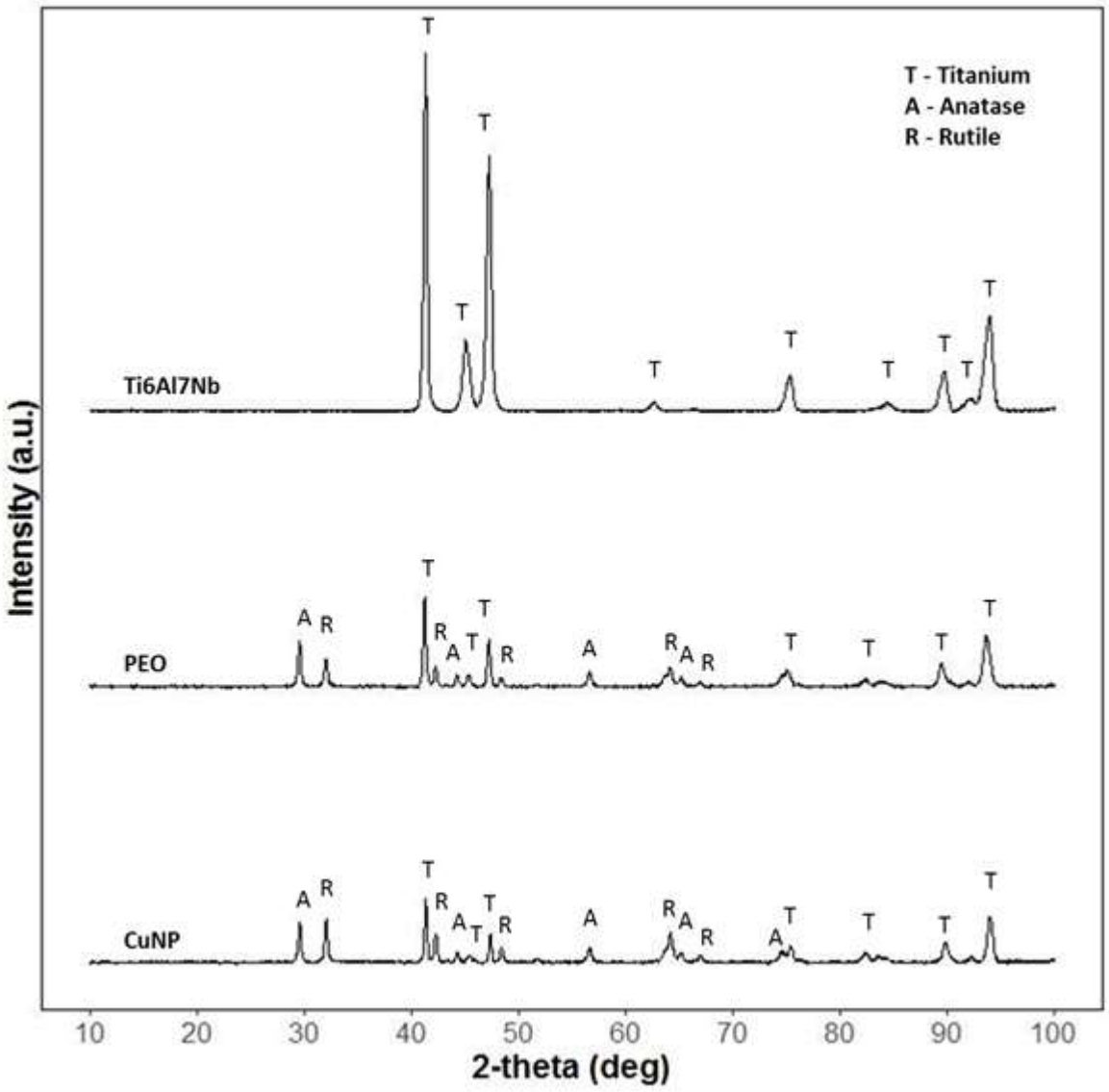

Figure 3.7. XRD patterns for Ti6Al7Nb alloy showing presence of Ti phase, PEO treated samples with TiO_2 and CuNP TiO_2 layers respectively show presence of anatase and rutile phases in addition to Ti phase.

3.4. Cu and Ag ion release

ICP-OES is an analytical technique used to detect trace metals. This technique was used to determine the concentration of Cu^{2+} and Ag ions (Ag^{+}) released from the CuNP and AgNP discs respectively into the PBS medium. The measurements were made at various time points over a period of 60 days and the results were analysed, calculations made and data presented as a cumulative release curve (Fig. 3.8). It is clear that under the same conditions, Ag^{+} are released from the PEO treated surface at a higher rate than Cu^{2+}. After 30 days, AgNP surface had released almost 150% more ions than the CuNP surface. The variation in the amount of Cu^{2+} released from each of three surfaces tested is also higher compared to the variation in the amount of Ag^{+} release from each of three AgNP surfaces tested. This is evidenced by the higher standard deviation of the mean of each time point for Cu^{2+} measured. It is also evident that after 30 days till 60 days there was an almost negligible release of Cu^{2+} amounting to 0.00446 ppm. In contrast, during the same period Ag^{+} continued to be released from the surface as revealed by the upward trend of the graph between the 30 and 60 day time points.

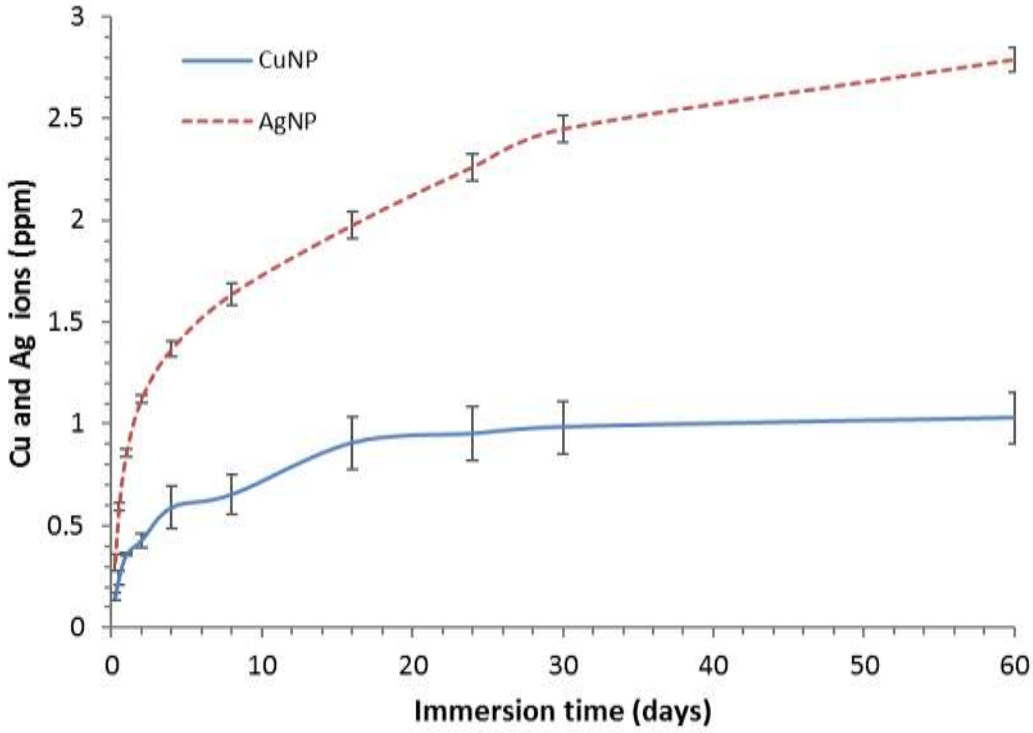

Figure 3.8. Cumulative release of Cu^{2+} and Ag^{+} from TiO_2 layers into a medium of PBS kept at 37º C. The Cu^{2+} and Ag^{+} released were measured at various time points over a period of 60 days. The data is expressed as means ± standard deviations (n = 3).

3.5. *In vitro* evaluation of antibacterial activity

3.5.1 Direct contact assay

The surface antibacterial activity of the PEO, CuNP and AgNP discs was evaluated using a direct contact assay called JIS test. The PEO surface free of Cu nanoparticles was used as a negative control and AgNP discs served as a positive control since the antibacterial activity of Ag nanoparticles is well established [26]. Figs. 3.9 and 3.10 are bar graphs showing the number of CFU of *S. aureus* and MRSA respectively present on the PEO, CuNP and AgNP layers. Calculations were made based on the quantitative cultures of *S.aureus* (Fig. 3.11) and MRSA (Fig. 3.13) solutions collected after sonication of the discs, which had been earlier inoculated and incubated for 24 hours. Also the cultures of the *S. aureus* and MRSA pellets obtained from the left over sonicated liquid of each bacterial strain were taken into consideration. Bacterial pellets of *S. aureus* and MRSA plated in total on blood agar showed no growth of bacteria after incubation for 24 hours (Figs. 3.12 and 3.14). Therefore, based on the quantitative cultures and pellet cultures, complete killing (100%) of the MRSA and *S. aureus* was found. The PEO layers without any Cu or Ag nanoparticles showed no bactericidal or bacteriostatic properties as evidenced by an approximately 430-fold increase in *S. aureus* CFU (bacteria increased from 4.05×10^4 CFU in the inoculum to 1.75×10^7 CFU after incubation for 24 hours) and an approximately 400-fold increase in MRSA CFU (bacteria increased from 3.75×10^4 CFU in the inoculum to 1.52×10^7 CFU after incubation for 24 hours). Based on the statistical analysis there was a significant effect of type of surface on the *S. aureus* and MRSA CFU. The difference between the effects of bacterial species on different surfaces was found to be not significant.

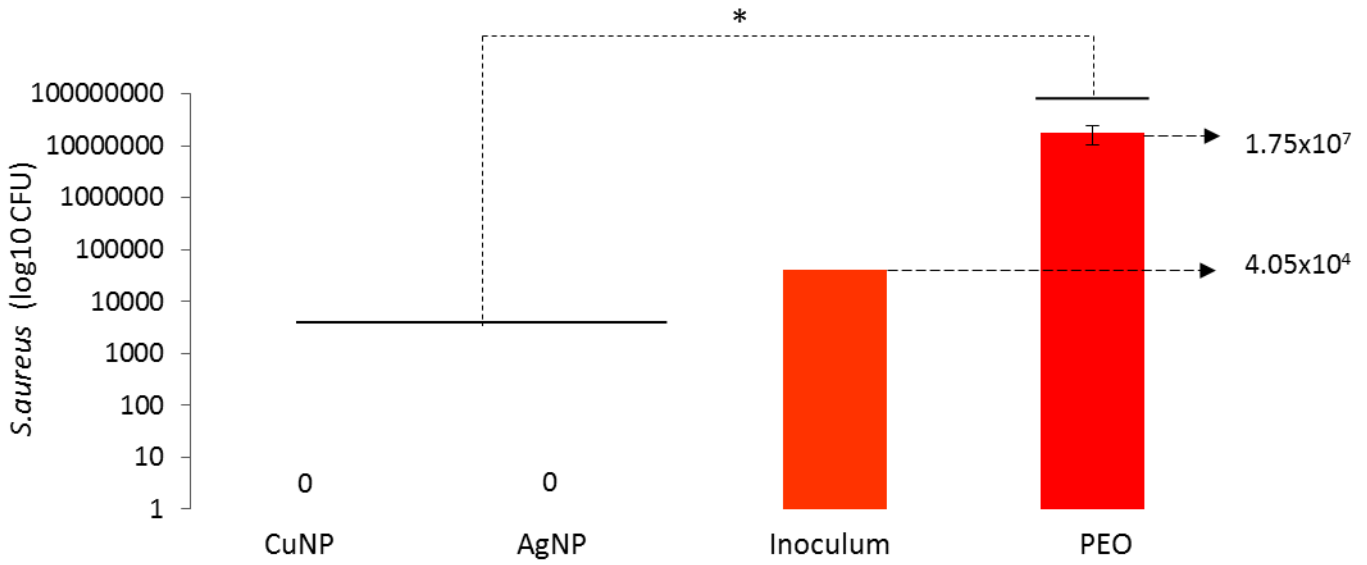

Figure 3.9. Amount of bacteria (CFU) in quantitative cultures of *S.aureus* present on PEO, CuNP and AgNP samples following 24 hours of incubation after inoculation (inoculum shown for reference). The data are expressed as means ± standard deviations (n = 3). Two-way ANOVA followed by Tukey post hoc test is utilized to determine the level of significance. $*p < 0.05$.

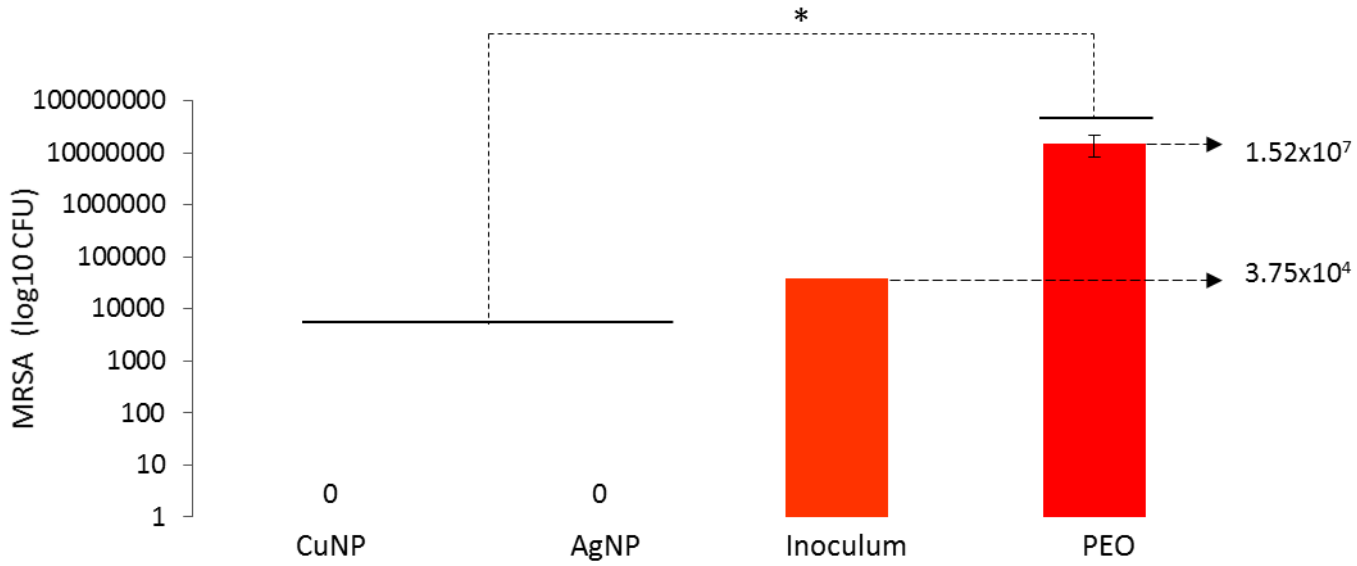

Figure 3.10. Amount of bacteria (CFU) in quantitative cultures of MRSA present on PEO, CuNP and AgNP samples following 24 hours of incubation after inoculation (inoculum shown for reference). The data are expressed as means ± standard deviations (n = 3).Two-way ANOVA followed by Tukey post hoc test is utilized to determine the level of significance. $*p < 0.05$.

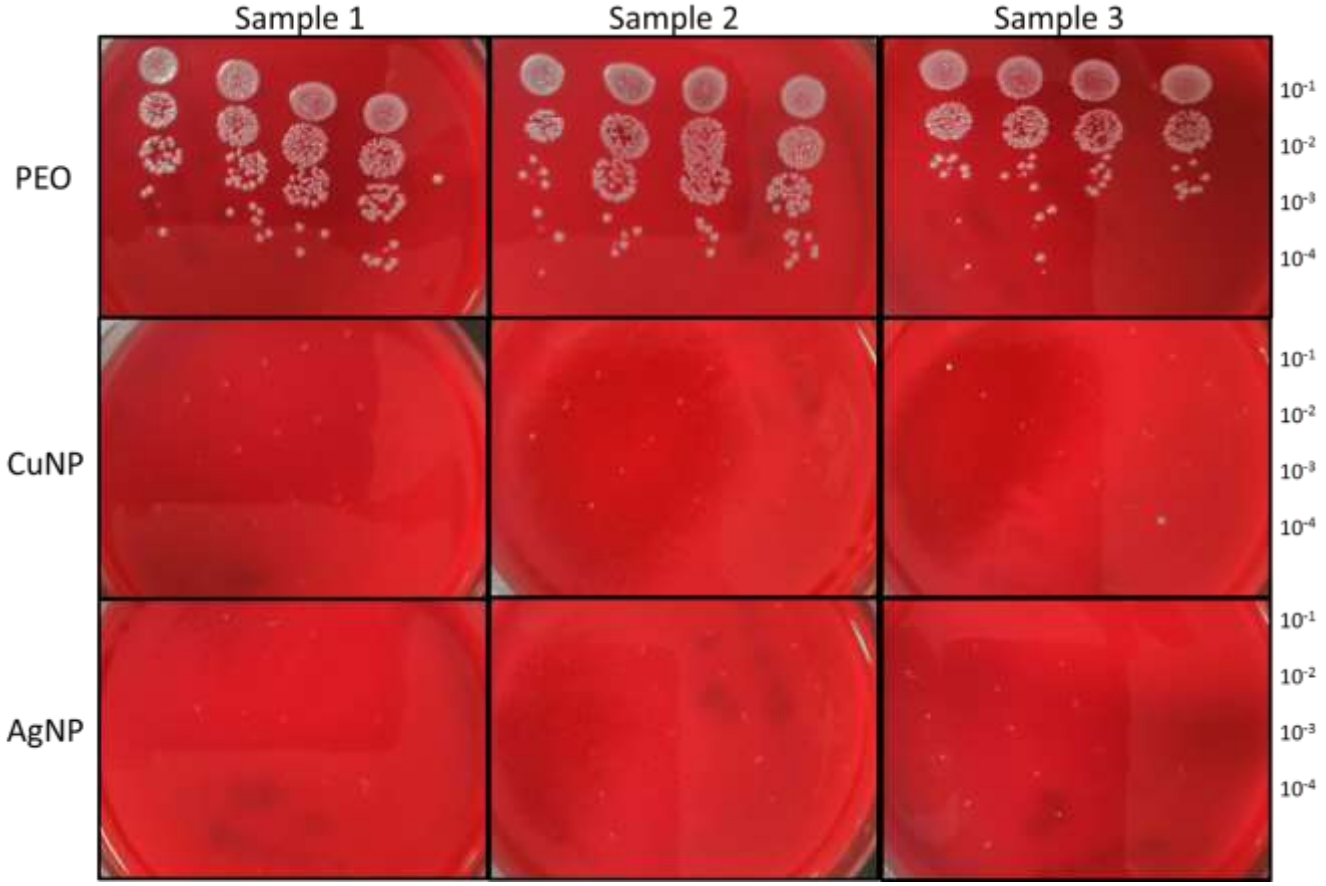

Figure 3.11. Quantitative cultures of *S.aureus* (RN4220) in triplicate after 24 hours incubation for PEO, CuNP and AgNP samples. PEO samples (free of Cu or Ag nanoparticles) showed a 430-fold increase in bacterial growth on their surface while CuNP and AgNP samples showed complete killing of bacteria.

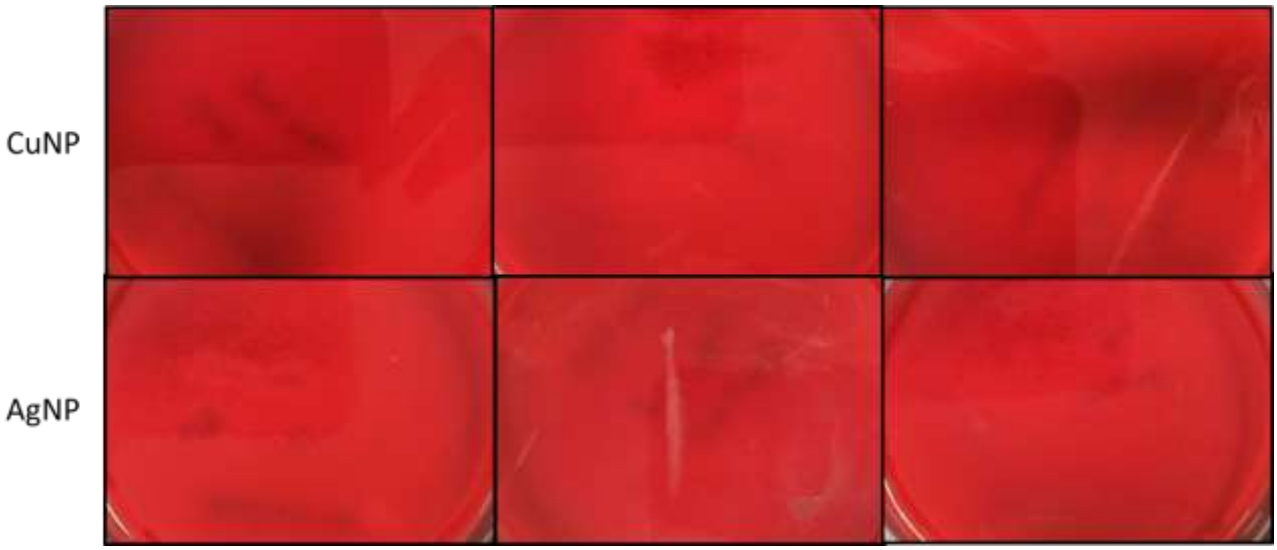

Figure 3.12. Cultures of *S.aureus* (RN4220) pellets in triplicate plated whole after 24 hours of incubation for CuNP and AgNP samples. Both samples showed complete killing of bacteria.

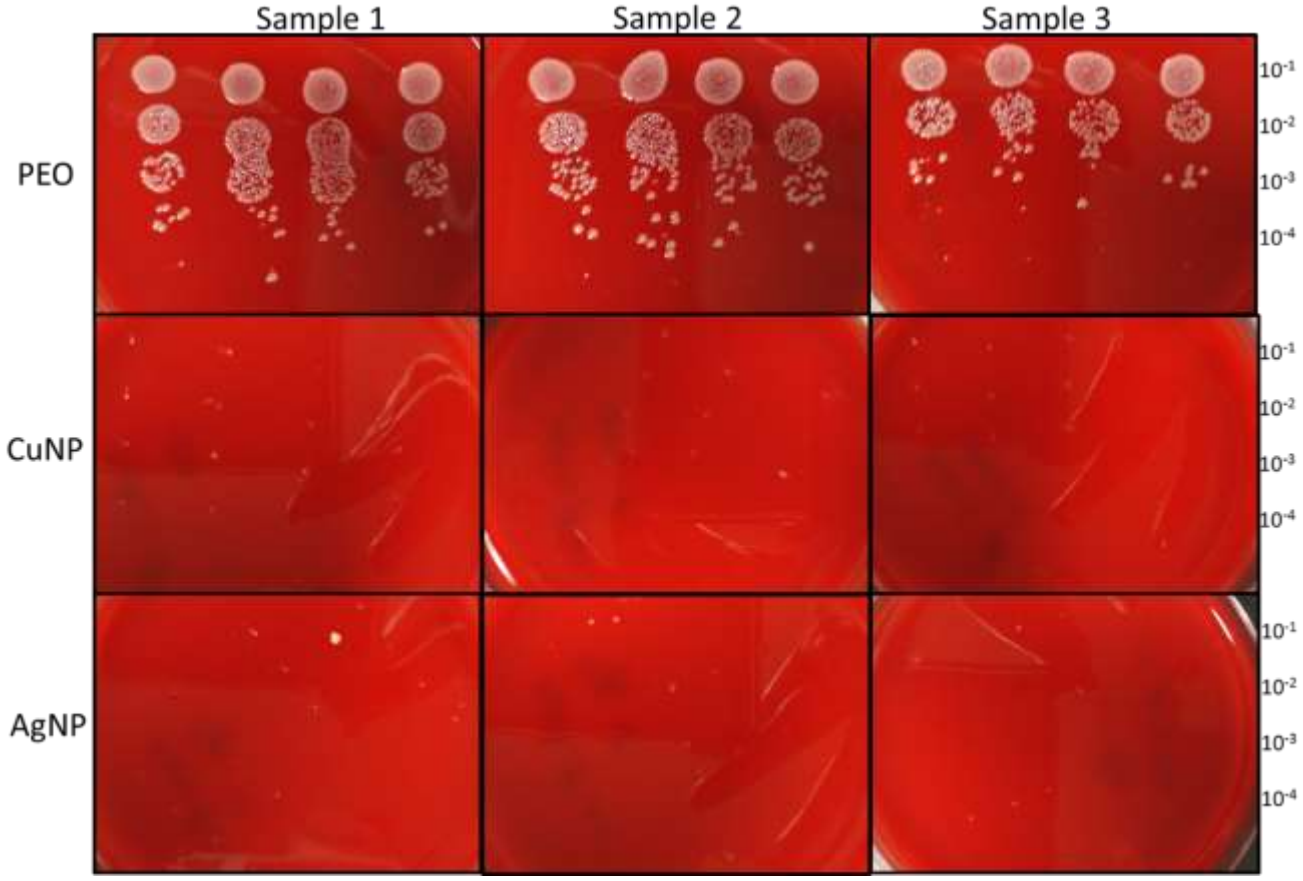

Figure 3.13. Quantitative cultures of MRSA (AMC201) in triplicate after 24 hours of incubation for PEO, CuNP and AgNP samples. PEO samples (free of Cu or Ag nanoparticles) showed a 400-fold increase in bacterial growth on their surfaces while CuNP and AgNP samples showed complete killing of bacteria.

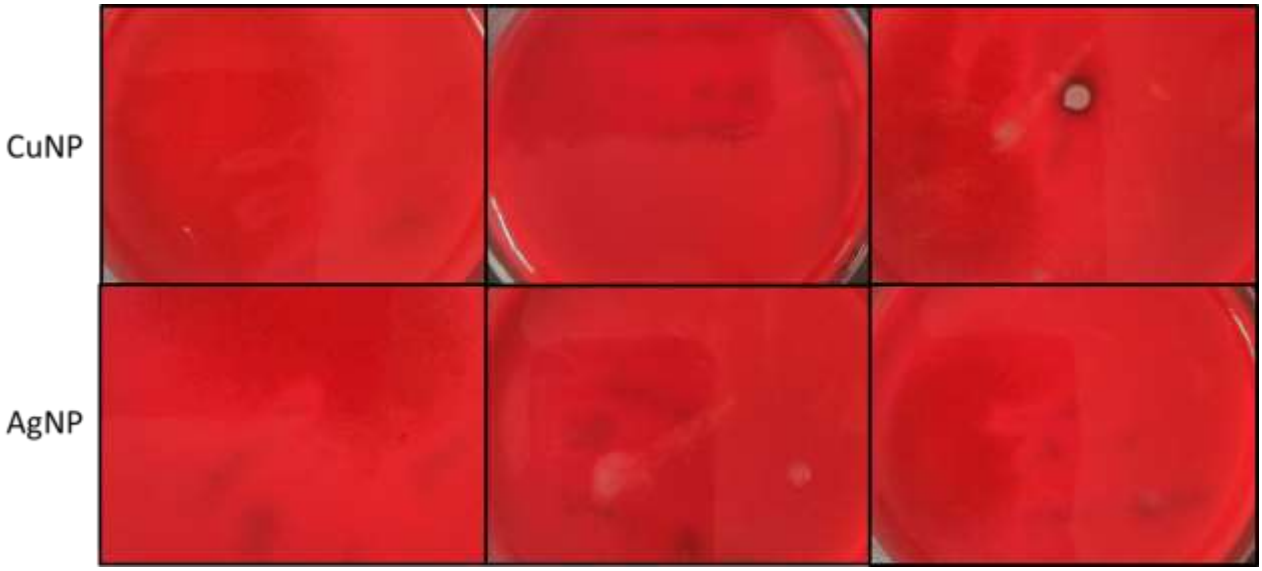

Figure 3.14. Cultures of MRSA (AMC201) pellets in triplicate plated whole after 24 hours of incubation for CuNP and AgNP samples. Both samples showed complete killing of bacteria.

3.5.2 Agar diffusion assay

The agar diffusion assay also called Kirby–Bauer test is generally used to establish the sensitivity of bacteria to different types of antibiotics. This assay was used to test the sensitivity of *S. aureus* to Cu-bearing disc surfaces. If leached Cu^{2+} from the CuNP surface inhibits bacterial growth or kills the bacteria, there will be an area around the disc where the bacteria have not grown enough to be visible. This is called a zone of inhibition.

Fig. 3.15 presents the results of the assay showing the growth inhibition zones (if present) around PEO, CuNP and AgNP discs. The CuNP surface has a circular bacterial growth inhibition zone measuring approximately 3 cm in diameter (Fig. 3.15b). It is assumed that Cu eluted from the surface of the disc inhibited the growth of bacteria in this zone. The PEO disc which served as a negative control showed no sign of bacterial inhibition in the form of a growth inhibition zone around it (Fig. 3.15a). The AgNP disc which serves as a positive control, has a growth inhibition zone clearly visible around the disc measuring approximately 3.1 cm in diameter (Fig. 3.15c). Even though the inhibition zones of both CuNP and AgNP are approximately equal in diameter, there is a clear difference in the respective appearance of the zones. The zone around the AgNP disc is clear with a distinctive border while the inhibition zone around CuNP is a bit faint and cloudy without a distinctive border, probably indicating that the bacterial inhibition by the AgNP surface is stronger than that of the CuNP surface at the bacterial concentration tested.

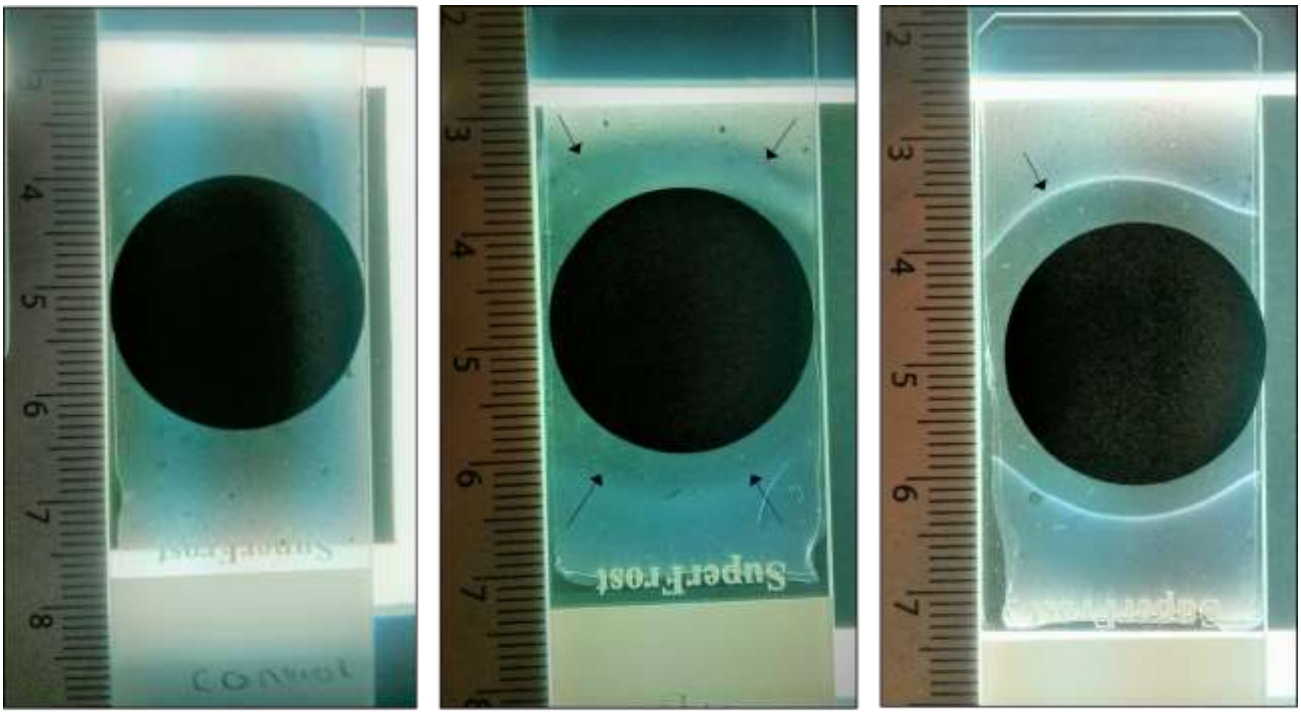

Figure 3.15. Growth inhibition zones of *S.aureus* due to leachable antibacterial activity of Cu-bearing layers, Ag-bearing layers (positive control) and PEO (negative control) after 24 hours of incubation. There was no inhibition zone visible around the PEO disc (a). A faint growth inhibition zone was formed around the CuNP disc after leaching of Cu^{2+} from the layers into the agar (indicated by arrows) (b). The growth inhibition zone formed around the AgNP disc is clear and distinct (c).

4 Discussion

Antibacterial surfaces are one of the promising strategies being studied to prevent IAI. Various materials are being investigated to find appropriate antibacterial agents which can be incorporated into a biomaterial surface. An ideal antibacterial surface is biocompatible and non-cytotoxic to host cells in addition to being antibacterial. Ag as a potential antibacterial agent has been researched and its antibacterial properties are well established [26] [35]. However, the main disadvantage of Ag is that it is cytotoxic even in small quantities. In the context of antibacterial implants which will be embedded inside the human body, Ag may cause damage to or kill human cells. An alternative inorganic material which is also well known for its antibacterial properties is Cu. Relatively less research has been done on Cu as an antibacterial agent for orthopaedic implant surfaces compared with Ag. Some studies suggest that in addition to displaying antibacterial properties, Cu preserves host cell viability and is potentially osteogenic and angiogenic [32] [33]. To demonstrate these properties, most studies tested for any cytotoxic effect of Cu against human cells by culturing human osteoblast cells on Cu-bearing surfaces. Cells were shown to proliferate over time and had well-formed and spread out morphology which is typical of healthy cells indicating that Cu could be non-cytotoxic. In addition, gene analysis showed that the presence of Cu stimulated the expression of genes such as osteogenic markers which were upregulated. Expression of vascular endothelial growth factor (VEGF) which is associated with angiogenesis was also upregulated. These results indicate that Cu could potentially be a favourable antibacterial agent in orthopaedic implant surfaces [33]. Moreover, Cu appears to be one of the few materials tested so far which can provide a balance between antibacterial activity against bacteria and cytotoxic effects on host cells [34][43].

Nanoparticles range in size from 1–100 nm and possess advantageous chemical, optical and mechanical properties. Due to their small size nanoparticles offer large surface area to volume ratio. For this reason metallic nanoparticles are suitable for use as potent antibacterial agents even in minute quantities [35]. Hence Cu nanoparticles were selected as the potential antibacterial agent for the purpose of the research carried out in this thesis. Various methods have been used in the literature to synthesise potential antibacterial surfaces comprising Cu nanoparticles with titanium alloys as substrate. PEO which is a versatile, environmentally friendly technique and delivers biomimetic surface layers was selected to synthesise Cu-bearing TiO_2 layers on Ti6Al7Nb biomedical alloy.

PEO generates a thick, porous, uniform and firmly adherent ceramic TiO_2 layer on the surface of Ti6Al7Nb. There is no noticeable variation in the porous morphology of Cu-free TiO_2 layers compared with Cu-bearing TiO_2 layers. The numerous plasma discharges create discharge channels which solidify into the characteristic porous morphology usually obtained by PEO (Figs 3.4 and 3.5). Cu nanoparticles, Ca and Phosphorus (P) get incorporated into the TiO_2 layers through these discharge channels by diffusion and other complex phenomena. A number of studies have shown that compounds of Ca and P play an important role in inducing osteogenesis i.e. bone formation [36] [37] [38]. For this reason, CA and CaGP were added to the electrolyte and subsequently Ca and P became integrated with the TiO_2 layers. Thus TiO_2 layers with embedded Cu nanoparticles, Ca and P perform a dual function of being antibacterial as well as osteoconductive. Highly rough and porous surfaces are known to be osteoconductive and play a role in osteogenesis [30]. Interconnected micro pores provide anchorage for bone cells leading to osteogenesis. In addition, complex porous geometry such as that synthesised by PEO is known to create niches in which bioactive materials such as growth factors and antibacterial agents can accumulate [31].

In addition to changes in surface morphology, the colour and appearance of the discs changed after treatment with PEO (Fig. 3.3). These changes in appearance could be related to the inclusion of Cu, Ag, Ca and P in their respective samples. The presence of these elements were assessed by analysing the surface chemistry of the TiO_2 layers of the samples.

SEM images of Cu-bearing TiO_2 layers at 10,000x magnification revealed the presence of particles on the TiO_2 surfaces in SED mode and light spots in BSE mode. EDS works on the principle that every element is associated with a unique electromagnetic emission spectra. The EDS spectra of Cu-bearing TiO_2 layers at various areas on the surface all indicated the presence of Ti, O, Al, Ca, P and Nb elements (Fig. 3.6). The intensity of the peaks were similar for different areas on the TiO_2 surface. However, the EDS spectra showed a few peaks corresponding to Cu when an area with particles was analysed (Fig. 3.6 (a and b)). The two spots “a” and “b” which were analysed due to presence of particles has more or less identical EDS spectra and indicated the presence of Cu. EDS analysis was also useful in verifying that Ca and P were incorporated into the Cu-bearing TiO_2 layers by the presence of Ca and P peaks. Some studies suggest that Ag nanoparticles as well as other types of nanoparticles become embedded inside micro pores in addition to the surface of the oxide layers [20] [26]. Therefore it is possible that Cu nanoparticles become embedded deep inside the multitude of pores on the TiO_2 surface.

XRD analysis was also used to characterise the surface of the Cu-bearing TiO_2 layers. In addition to the elements present in the Cu-bearing TiO_2 layers, it is interesting to understand the crystalline phases present since studies have shown that the phases of TiO_2 i.e. anatase and rutile are known to exhibit antibacterial properties [39] [40]. As expected, peaks of intensity which correspond to anatase and rutile phases of TiO_2 were identified from their characteristic intensity peaks for Cu-free TiO_2 layers as well as Cu-bearing TiO_2 layers (Fig. 3.7). Another phase also detected was of Ti. Most of the peaks in the XRD pattern corresponded to the Ti phase, this is because the bulk of the substrate is made up of Ti.

A crucial factor which could catapult Cu as the most desirable antibacterial agent is if it provides evidence of a clear antibacterial effect without being cytotoxic to host cells, as already mentioned. A critical factor which affects this balance is the concentration of Cu^{2+} released from the surface into its immediate environment. In the scenario of an implant inside the human body, Cu^{2+} released into its microenvironment will interact with bacteria, blood cells, plasma and human tissue cells. If the concentration of Cu^{2+} released is too high, it may damage host cells, but if Cu^{2+} concentration is too low, it may be ineffective against bacteria. In the ICP-OES analysis of Cu^{2+} and Ag^{+} released from respective disc surfaces, it is immediately apparent that Ag^{+} are released at a significantly higher rate compared with Cu^{2+} released (Fig.3.8). The reason for these differences in release rate is not immediately clear but may have to do with the unique properties of Ag and Cu and their distinctive atomic structures. Another possibility is that more Ag nanoparticles were incorporated into the AgNP surfaces than were Cu nanoparticles into CuNP surfaces leading to a higher concentration of Ag^{+} released from the surface, but this has not been verified. Both Cu^{2+} and Ag^{+} were released in a prolonged and sustained manner over a relatively long period of 60 days. This release profile is beneficial because a sustained release will provide an antibacterial activity, if any, over a longer duration. In the scenario of IAI, in the few weeks following surgery the patient is most susceptible to infections due to a weakened immune system and it is during this time that antibacterial agents must compensate. A release profile which shows a burst of ions released initially but quickly diminishes is unfavourable in the scenario of antibacterial surfaces.

Cu in very small quantities acts as a micronutrient to bacteria. In an experiment which tested the antibacterial activity of Cu nanoparticles dispersed in deionised water against *Escherichia coli* (*E. coli*), 60 µg/mL of Cu nanoparticles was the lowest concentration at which all bacteria were killed [45]. It appears that the Cu concentration in liquid medium has a significant effect on bacteria. A very low concentration of Cu may even be beneficial to bacterial while higher Cu concentrations are detrimental to their survival. The natural question is what is the value of an appropriate Cu^{2+} concentration in solution? One study found that a Cu^{2+} concentration of 10.85 ppm (mg/L) induces cytotoxicity in Chinese hamster cells [41]. In the ICP-OES analysis performed for this research 0.3595 ppm of Cu^{2+} was released after the first 24 hours (Fig.3.8) which is well below this cytotoxicity threshold of 10.85 ppm. In another similar study, Cu-bearing surfaces were synthesised by plasma immersion ion implantation and deposition (PIII&D) and the Cu released from the surface into PBS medium was measured by ICP-OES and found to be 0.0636ppm after 24 hours [32]. This is well below the Cu^{2+} concentration of 0.3595 ppm for Cu-bearing samples prepared by PEO used in the present study. Therefore it appears that the release of higher Cu^{2+} concentrations of a few ppm may not be detrimental to host cells.

Other than the effect of Cu on host cells, it is important to establish that Cu nanoparticles demonstrate antibacterial activity against bacteria. It is clear from the literature that the antibacterial activity of metallic nanoparticles varies based on the bacterial species it is tested against [42].For this reason the surface bactericidal activity of Cu layers was assessed against two bacterial species. *S. aureus* which is the most common cause of IAI and MRSA which is one of the most prevalent and virulent pathogens responsible for IAI. A direct contact assay was used to evaluate the surface antibacterial activity of Cu-bearing TiO_2 layers. The direct contact assay allows a quantitative interpretation of bactericidal activity based on killing of a defined inoculum. All 4.05 x 10^4 CFU of *S. aureus* and 3.75 x 10^4 CFU of MRSA respectively, seeded on Cu layers, were completely killed in 24 hours (Figs. 3.9, 3.10, 3.11 and 3.13). However, the detection limit of the assay is 500 CFU. This means that 500 CFU in 5 mL (which was the total volume of the sonicated solution) will not be culturable in 10 µL. Therefore, the percent of bacteria killed is reported to be 99.75% and not 100%. To improve the detection limit to 100%, bacterial pellets made from the remaining liquid sonicate was plated as a whole. No bacteria grew after 24 hours of incubation for both bacterial species (Figs. 3.12 and 3.14). Therefore it can be reported that 100% of *S. aureus* and MRSA were killed in the presence of Cu nanoparticles. The Cu-free samples were found to be neither bactericidal nor bacteriostatic. Thus, the antibacterial activity of Cu-bearing TiO_2 layers should be attributed to the Cu nanoparticles incorporated in these layers because Cu-free layers showed no bactericidal activity.

A number of studies indicate that an increase in Cu concentration in the antibacterial surface kills a larger number of bacteria [43] [44] [45] [46]. It is further suggested that *S.aureus* and MRSA (and possibly other bacterial species) tolerate a certain amount of Cu until a distinct threshold concentration is reached, followed by a significant and disproportionate drop in CFU [43] [44]. However, most of these studies did not report complete killing of bacteria when tested with Cu-bearing TiO_2 surfaces. This may be due to several factors such as an insufficient concentration of Cu in the antibacterial surface tested. Moreover, the methods by which Cu-bearing surfaces are synthesised may have an impact on the rate of Cu^{2+} release, the concentration of Cu^{2+} released etc. and in turn affect the antibacterial activity of the surfaces.

An agar diffusion assay was used to assess the leachable antibacterial activity and possible surface antibacterial activity as well. The Cu^{2+} and Ag^{+} released into the agar creates a bacterial growth inhibition zone around the respective discs (Figs. 3.15). The zone of inhibition around the Cu-bearing TiO_2 disc was cloudy and faint indicating that growth inhibition of bacterial in the zone was not complete Figs. 3.15b. If complete inhibition of bacterial growth had occurred, the zone would have been clear like the Ag^{+} positive control Figs. 3.15c. It is possible that the Cu concentration in the Cu-bearing disc was low, leading to weak leaching into the agar. These results are in line with another study in which Cu^{2+} released from Ti-Cu alloy surfaces did not show a distinct zone of inhibition when an agar diffusion assay was performed [47].

From the results of this study it is clear that Cu-bearing TiO_2 layers display antibacterial activity. However not much is known on a molecular level about the mechanisms by which Cu kills bacteria. An atomic force microscopy study of bacteria after contacting a Cu-bearing surface revealed that the structure of the outer membrane responsible for cell permeability was substantially altered. The cell walls were seriously damaged and contents of the cells had leaked out. It is further suggested in some studies that electrostatic forces between Cu^{2+} and gram-negative bacteria is an important factor for bacterial killing [48]. Studies regarding the mechanism of Ag killing state that the interaction of Ag with microbial cells causes degradation of lipopolysaccharide molecules on the outer membrane leading to pit formation and large increases in membrane permeability [49]. Cu and Ag may also produce secondary products such as reactive oxygen species (ROS) that penetrate bacterial cell walls and cause damage to DNA and protein oxidation [50].

5 Recommendations for future work

Based on the results of this research, the antibacterial activity of Cu-bearing TiO_2 surfaces looks promising and future research is worth pursuing. Below are mentioned some recommendations for future research and experiments:

- The Cu-bearing TiO_2 surfaces can be further characterised to understand more about this surface. The surface roughness, wettability, surface free energy, porosity and pore size distribution can be studied and quantified.
- The amount of Cu present in the TiO_2 layers can be quantified. This data will be useful to draw a relationship between the concentration of Cu nanoparticles incorporated from the electrolyte into the layers and the Cu^{2+} released from the surface by leaching. If these values are known, it will be possible to fine tune the Cu concentration to have a balanced antibacterial activity without cytotoxicity.
- The concentration of CFU in the bacterial inoculum of both bacterial strains tested in the direct contact assay can be increased and inoculum with different concentrations of CFU can be tested. The limits of Cu and Ag bactericidal activity can be explored.
- The agar diffusion assay can be performed with higher concentrations of leached Cu^{2+} and quantification of the zone of inhibition can be performed and bacteriostatic and bactericidal effect of leached Cu assessed, if any.
- Since multiple bacterial species cause IAI, antibacterial activity of Cu bearing layers against species such as *Staphylococcus Epidermidis* can be tested.
- Investigate further the release rate of Cu^{2+} from the Cu-bearing layers in a medium which mimics *in vivo* conditions better such as use of human plasma in the medium.
- Assays to assess the cytotoxicity of the Cu-bearing TiO_2 layers on human osteoblast cells can be performed.

6 Conclusions

Cu-bearing TiO_2 layers were successfully synthesised on a Ti6Al7Nb biomedical alloy using PEO in an electrolyte with a concentrations of 3.0 g/L Cu nanoparticles, CA and CaGP added. The layers were characterized with respect to surface morphology, chemical composition and phase composition. All layers presented a porous morphology, with pore sizes ranging from a few nm up to a few µm. The presence of Cu, Ca and P in the Cu bearing TiO_2 layers were identified. The phases present in TiO_2 layers were found to be anatase and rutile. Except for the presence of Cu nanoparticles, the main surface characteristics remained unchanged in the Cu-bearing TiO_2 layers compared with the Cu-free TiO_2 layers. Cu^{2+} released into PBS medium from Cu-bearing TiO_2 layers showed a sustained release over sixty days.

The *in vitro* antibacterial activity of the TiO_2 surfaces bearing Cu nanoparticles against *S. aureus* and MRSA was investigated. A direct contact assay was used to assess the surface antibacterial activity and showed complete killing of both bacterial species in 24 hours. The direct contact of bacteria with the Cu-bearing surfaces may have strongly contributed to the complete killing of bacterial CFU. The Cu-free samples showed an exponential increase in bacterial CFU. The agar diffusion assay demonstrated the leaching antibacterial activity of the Cu-bearing layers against *S.aureus*. Within 24 hours, a faint growth inhibition zone was observed around Cu-bearing samples presumably due to the bacteriostatic effect of released Cu^{2+} into the surrounding agar. The results of the antibacterial assays together with the Cu^{2+} release rate helped explain the potential bactericidal mechanism of Cu-bearing layers. A dual antibacterial mechanism was proposed, as both direct contact of Cu nanoparticles per se as well as the release of Cu^{2+} into its surroundings, contribute to the antibacterial activity of the Cu-bearing TiO_2 layers.

Acknowledgements

I am deeply grateful to my mentor Dr. ir. Iulian Apachitei from TU Delft for giving me the opportunity to work on a challenging and extremely interesting research project. Due to his constant guidance and knowledge I have learnt a lot while working with this project. I thank Michel van den Brick from the TU Delft Process and Energy department for helping me with the ICP-OES analysis and Ruud Hendrikx from 3ME for helping me with the XRD analysis. I thank Sander Leeflang for supervising me and helping me with practical matters in the Biomaterials laboratory.

I specially thank the staff at Academic Medical Centre (AMC), Amsterdam for their helpfulness and patience during my time at AMC where I worked on the antibacterial studies. In this regard, I thank Dr. S.A.J. Zaat from the AMC staff, Martijn Riool who resolved all my questions regarding biological assays and Leonie de Boer for being very attentive and helpful in the microbiology laboratory. I also thank Dr. ir. Amir Zadpoor from Biomedical Engineering for his support during completion of the research. I thank my fellow students Devina Varieth and Ingmar Van Hengel for their collaboration and assistance during the many hours spent at the biomaterials laboratory.

Lastly I am very grateful to my parents, sisters, Ragunath Sivakumaran and many other friends and fellow students at TU Delft for their unstinting support, encouragement and love which helped me through the months spent to complete the research.

References

[1] Wittenauer, Rachel, Lily Smith, and Kamal Aden. "Background Paper 6.12 Osteoarthritis." Geneva, Switzerland: World Health Organization (2013).
[2]Rankin, E. Anthony, et al. "NIH Consensus Statement on total knee replacement December 8-10, 2003." Journal of Bone and Joint Surgery 86.6 (2004): 1328.
[3] https://www.hss.edu/conditions_whats-new-in-cartilage-repair.asp
[4] Shanbhag, Arun, Harry E. Rubash, and Joshua J. Jacobs. "Joint Replacement and Bone Resorption." Pathology, Biomaterials, and Clinical Practice: Taylor & Francis (2006): 331-344.
[5] Kapadia, Bhaveen H., et al. "Periprosthetic joint infection." The Lancet 387.10016 (2016): 386-394.
[6] Bozic, Kevin J., et al. "The epidemiology of revision total knee arthroplasty in the United States." Clinical Orthopaedics and Related Research® 468.1 (2010): 45-51.
[7]https://mykneereplacementjournal.wordpress.com/
[8] http://www.gponline.com/complications-total-knee-replacement-surgery/musculoskeletal-disorders/rheumatoid-arthritis-other-autoimmune-disorders/article/1209527
[9] Campoccia, Davide, Lucio Montanaro, and Carla Renata Arciola. "The significance of infection related to orthopedic devices and issues of antibiotic resistance." Biomaterials 27.11 (2006): 2331-2339.
[10] F. Paladini, M. Pollini, A. Sannino and L. Ambrosio, Metal-based antibacterial substrates for biomedical applications, Biomacromolecules 16.7 (2015): 1873-1885.
[11] T. Böttcher, I. Kolodkin-Gal, R. Kolter, R. Losick, J. Clardy, Synthesis and Activity of Biomimetic Biofilm Disruptors, J Am Chem Soc. 2013 Feb 27; 135(8): 2927–2930.
[12] Cattelan, Natalia, et al. "Bordetella biofilms: a lifestyle leading to persistent infections." Pathogens and disease 74.1 (2016): ftv108.
[13] Follmann, Heveline DM, et al. "Antiadhesive and antibacterial multilayer films via layer-by-layer assembly of TMC/heparin complexes." Biomacromolecules 13.11 (2012): 3711-3722.
[14] Muszanska, Agnieszka K., et al. "Antiadhesive polymer brush coating functionalized with antimicrobial and RGD peptides to reduce biofilm formation and enhance tissue integration." Biomacromolecules 15.6 (2014): 2019-2026.
[15] Poncin-Epaillard, F., et al. "Elaboration of highly hydrophobic polymeric surface—a potential strategy to reduce the adhesion of pathogenic bacteria?." Materials Science and Engineering: C 33.3 (2013): 1152-1161.
[16] Ivanova, Elena P., et al. "Impact of nanoscale roughness of titanium thin film surfaces on bacterial retention." Langmuir 26.3 (2009): 1973-1982.
[17] A. Gristina, P. Naylor, Q. Myrvik, Infections from biomaterials and implants: a race for the surface, Medical progress through technology 14.3-4 (1987): 205-224.
[18] Gallo, Jiri, Martin Holinka, and Calin S. Moucha. "Antibacterial surface treatment for orthopaedic implants." International journal of molecular sciences 15.8 (2014): 13849-13880.
[19] Tan, Honglue, et al. "Quaternized chitosan as an antimicrobial agent: Antimicrobial activity, mechanism of action and biomedical applications in orthopedics." International journal of molecular sciences 14.1 (2013): 1854-1869.
[20] Mei, Shenglin, et al. "Antibacterial effects and biocompatibility of titanium surfaces with graded silver incorporation in titania nanotubes." Biomaterials 35.14 (2014): 4255-4265.
[21]Haenle, Maximilian, et al. "An extended spectrum bactericidal titanium dioxide (TiO_2) coating for metallic implants: in vitro effectiveness against MRSA and mechanical properties." Journal of Materials Science: Materials in Medicine 22.2 (2011): 381-387.
[22] Mijnendonckx, Kristel, et al. "Antimicrobial silver: uses, toxicity and potential for resistance." Biometals 26.4 (2013): 609-621.
[23] S.G. Steinemann, S.M. Perren, Surgical implant and alloy for use in making an implant,US Patent 4040129, 9 Aug 1977.
[24] Titanium processing. (2016). In Encyclopædia Britannica. Retrieved from https://www.britannica.com/technology/titanium-processing
[25] http://ssnano.com/inc/sdetail/copper_nanoparticles/267
[26] B. Necula, Silver-based antibacterial surfaces for bone implants, PhD Thesis, T U Delft repository, November 2013
[27] http://www.sigmaaldrich.com/catalog/product/aldrich/730793?lang=en&region=NL
[28] JIS Z 2801:2000 Antimicrobial Products – Test for antimicrobial activity and efficacy
[29] Yerokhin, A. L., et al. "Plasma electrolysis for surface engineering." Surface and Coatings Technology 122.2 (1999): 73-93.
[30] Sul, Young-Taeg. "The significance of the surface properties of oxidized titanium to the bone response: special emphasis on potential biochemical bonding of oxidized titanium implant." Biomaterials 24.22 (2003): 3893-3907.
[31] Necula, B. S., et al. "Titanium bone implants with superimposed micro/nano-scale porosity and antibacterial capability." Applied Surface Science 273 (2013): 310-314.

[32] Yu, Le, et al. "Antibacterial activity, osteogenic and angiogenic behaviors of copper-bearing titanium synthesized by PIII&D." Journal of Materials Chemistry B 4.7 (2016): 1296-1309.
[33] Wu, Qianju, et al. "Antibacterial property, angiogenic and osteogenic activity of Cu-incorporated TiO_2 coating." Journal of Materials Chemistry B 2.39 (2014): 6738-6748.
[34] Norambuena, German A., et al. "Antibacterial and Biocompatible Titanium-Copper Oxide Coating May Be a Potential Strategy to Reduce Periprosthetic Infection: An In Vitro Study." Clinical Orthopaedics and Related Research® (2016): 1-11.
[35] Rai, Mahendra, Alka Yadav, and Aniket Gade. "Silver nanoparticles as a new generation of antimicrobials." Biotechnology advances 27.1 (2009): 76-83.
[36] Song, Won-Hoon, et al. "Biomimetic apatite coatings on micro-arc oxidized titania." Biomaterials 25.17 (2004): 3341-3349.
[37] Fujibayashi, Shunsuke, et al. "Osteoinduction of porous bioactive titanium metal." Biomaterials 25.3 (2004): 443-450.
[38] Surmenev, Roman A., Maria A. Surmeneva, and Anna A. Ivanova. "Significance of calcium phosphate coatings for the enhancement of new bone osteogenesis–A review." Acta biomaterialia 10.2 (2014): 557-579.
[39] Fu, Guifen, Patricia S. Vary, and Chhiu-Tsu Lin. "Anatase TiO_2 nanocomposites for antimicrobial coatings." The Journal of Physical Chemistry B 109.18 (2005): 8889-8898.
[40] Caratto, V., et al. "Inactivation of Escherichia coli on anatase and rutile nanoparticles using UV and fluorescent light." Materials Research Bulletin 48.6 (2013): 2095-2101.
[41]Grillo, C. A., M. A. Reigosa, and M. Fernández Lorenzo de Mele. "Effects of copper ions released from metallic copper on CHO-K1 cells." Mutation Research/Genetic Toxicology and Environmental Mutagenesis 672.1 (2009): 45-50.
[42] Ruparelia, Jayesh P., et al. "Strain specificity in antimicrobial activity of silver and copper nanoparticles." Acta biomaterialia 4.3 (2008): 707-716.
[43] Heidenau, F., et al. "A novel antibacterial titania coating: metal ion toxicity and in vitro surface colonization." Journal of Materials Science: Materials in Medicine 16.10 (2005): 883-888.
[44] Haenle, Maximilian, et al. "An extended spectrum bactericidal titanium dioxide (TiO_2) coating for metallic implants: in vitro effectiveness against MRSA and mechanical properties." Journal of Materials Science: Materials in Medicine 22.2 (2011): 381-387.
[45] Polak, Martin, et al. "Oxygen and Water Plasma-Immersion Ion Implantation of Copper into Titanium for Antibacterial Surfaces of Medical Implants." Advanced Engineering Materials 12.9 (2010): B511-B518.
[46] Raffi, Muhammad, et al. "Investigations into the antibacterial behavior of copper nanoparticles against Escherichia coli." Annals of Microbiology 60.1 (2010): 75-80.
[47] Zhang, Erlin, et al. "A new antibacterial titanium–copper sintered alloy: preparation and antibacterial property." Materials Science and Engineering: C 33.7 (2013): 4280-4287.
[48] Nan, Li, et al. "Study on antibacterial mechanism of copper-bearing austenitic antibacterial stainless steel by atomic force microscopy." Journal of Materials Science: Materials in Medicine 19.9 (2008): 3057-3062.
[49] I. Sondi, B. Salopek-Sondi, Silver nanoparticles as antimicrobial agent: a case study on E-coli as a model for Gram-negative bacteria, Journal of Colloid and Interface Science, 275 (2004) 177-182.
[50] Applerot, Guy, et al. "Understanding the antibacterial mechanism of CuO nanoparticles: revealing the route of induced oxidative stress." Small 8.21 (2012): 3326-3337.